The Astronomical Journal, 129:160–177, 2005 January

DDO 88: A GALAXY-SIZED HOLE IN THE INTERSTELLAR MEDIUM

Caroline E. Simpson
Department of Physics, Florida International University, University Park, Miami, FL 33199; simpsonc@galaxy.fiu.edu

Deidre A. Hunter
Lowell Observatory, 1400 West Mars Hill Road, Flagstaff, AZ 86001; dah@lowell.edu

and

Patricia M. Knezek
WIYN Consortium, Inc., 950 North Cherry Avenue, Tucson, AZ 85726-6732; knezek@noao.edu
Received 2004 May 10; accepted 2004 September 28

ABSTRACT

We present an H I and optical study of the gas-rich dwarf irregular galaxy DDO 88. Although the global optical and H I parameters of DDO 88 are normal for its morphological type, it hosts a large (3 kpc diameter) and unusually complete ring of enhanced H I emission. The normal appearance of this galaxy in the optical and the outer regions of the H I give no hint of the presence of the striking H I ring in the inner regions. The gas ring is located at approximately one-third of the total H I radius and one-half the optically defined Holmberg radius, and contains 30% of the total H I of the galaxy. The ring surrounds a central depression in the H I distribution. If the H I ring and central depression in the gas were formed by the energy input from winds and supernova explosions of massive stars formed in a starburst, as is thought often to be the case, the star-forming event would have formed 0.1%–1% of the total stellar mass of the galaxy. However, the *UBV* colors in the H I hole are not bluer than the rest of the galaxy, as would be expected if an unusual star-forming event had taken place there recently, although there is an old (∼1–3 Gyr), red cluster near the center of the hole that is massive enough to have produced the hole in the H I. An age estimate for the ring is uncertain, however, because it is not observed to be expanding. An expansion model produces a lower estimate of 0.5 Gyr, but the presence of faint star formation regions associated with the ring indicates a much younger age. We also estimate that the ring could have dispersed by now if it is older than 0.5 Gyr. This implies that the ring is younger than 0.5 Gyr. A younger age would indicate that the red cluster did not produce the hole and ring. Therefore, uncertainties prevent us from concluding that the cluster and the H I hole are definitely related. If this ring and the depression in the gas that it surrounds were not formed by stellar winds and supernovae, this would indicate that some other, currently unidentified, mechanism is operating.

Key words: galaxies: individual (DDO 88) — galaxies: irregular — galaxies: ISM — galaxies: kinematics and dynamics — galaxies: photometry

1. INTRODUCTION

DDO 88 (=NGC 3377A, UGC 5889) is a gas-rich dwarf irregular galaxy located in the Leo I Group (M96). It came to our attention when 21 cm observations taken with the Very Large Array (VLA) radio telescope[1] indicated the presence of an apparent ring of H I surrounding the optical body of the galaxy (Simpson & Gottesman 2000). Although these data suffered from a lack of sensitivity, the suggestion of a large hole (∼2–3 kpc; $D = 7.4$ Mpc) in the H I distribution was intriguing. There are examples of other large holes in similar galaxies (Walter & Brinks 1999; Wilcots & Miller 1998; Puche et al. 1992; Sargent et al. 1983), but this seemed extreme.

Star formation episodes are thought to more strongly affect the interstellar medium (ISM) in low-mass galaxies and have been invoked to explain the presence of shells, holes, and filaments observed in small galaxies (e.g., Ott et al. 2001; Stewart et al. 2000; Walter & Brinks 1999; Martin 1998; Meurer et al. 1992, 1998; Young & Lo 1996; Puche et al. 1992; but see Rhode et al. 1999). Star formation in low-mass, slowly rotating galaxies appears to be regulated by the feedback between the energy deposited in the ISM by massive star formation and the ISM itself. Energy transferred from stellar winds and supernova events both heats up and disperses the ISM surrounding the star formation area (see, e.g., Scalo & Chappell 1999). It is thought that as the H I column density drops below a critical threshold necessary for star formation to occur, the star formation episode will switch off. Meanwhile, cold, dense material is swept up and compressed around the edges of the region, triggering further star formation. This effect should be particularly strong in low-mass systems such as dwarfs (Mac Low & Ferrara 1999; De Young & Heckman 1994).

To further investigate the interplay between star formation and the H I reservoir in irregular galaxies, we have obtained additional radio and optical observations of DDO 88. High-sensitivity VLA D-configuration and high-resolution CS-configuration 21 cm observations have been taken, along with *U*, *B*, *V*, *R*, *H*, and Hα images, as well as long-slit spectra. Here we present the results from this new H I and optical study.

2. OBSERVATIONS

2.1. H I

DDO 88 was observed using the D configuration of the VLA for a total of approximately 7.5 hr over 2 days and for approximately 2.5 hr using the CS configuration. Table 1 lists all

[1] The VLA is a facility of the National Radio Astronomy Observatory, operated by Associated Universities, Inc., under cooperative agreement with the National Science Foundation.

TABLE 1
VLA Observations

Parameter	D Configuration	CS Configuration	C+D[a]
Observation date	1996 Sep 20 and 24	1997 Sep 19	...
Time on source (minutes)	449	161	...
Bandwidth (MHz)	1.56	1.56	1.56
Channels	128	128	128
Velocity resolution (km s^{-1})	2.6	2.6	2.6
Beam size[b] (arcsec)	55.6×53.6	14.5×13.1	16.8×14.6
Single-channel rms (mJy $beam^{-1}$)	0.71	1.26	0.98

[a] Combined data set from both configurations.
[b] Natural weighting for D; uniform weighting with robust factor of −1 for CS and C+D.

the observational parameters for each data set. The D configuration provides numerous short spacings, resulting in high sensitivity but low (nominally 45″) resolution, while the CS configuration provides longer baselines and therefore higher resolution (nominally 12.″5), but with some loss in sensitivity.[2] All observations were made using a 128 channel spectrometer with a channel separation of 12.2 kHz (2.6 km s^{-1}), resulting in a total bandwidth of 1.56 MHz. The 2IF mode was used with online Hanning smoothing. The nearby continuum source 1117+146 (B1950) was used as a phase calibrator, with 1328+307 (B1950) used as a flux and bandpass calibrator for the D-configuration observations, and 0538+498 (J2000) used for the CS-configuration observations.

The observations were edited and calibrated using the standard routines in AIPS. There was solar interference present in all the data sets, primarily affecting the short baselines. The D-configuration observations were the most affected, with up to 20% of the data contaminated. For both the D and CS data the contaminated visibilities were flagged, and satisfactory solutions were subsequently obtained. The continuum emission was removed in the *u-v* plane using an average of emission-free channels on both sides of the galaxy spectrum.

The D-configuration data sets from each day were edited and calibrated separately, then combined in the *u-v* plane and Fourier-transformed using the AIPS task IMAGR to make a cube of images, one image for each frequency channel observed. Natural weighting was used to produce images with the greatest sensitivity to low-level emission. This image cube has a spatial resolution of $55.''59 \times 53.''56$, with a single-channel rms (σ) of 0.7 mJy $beam^{-1}$. During imaging, each channel was CLEANed (Clark 1980) to this level to remove the effects of the dirty beam. Channels containing signal in the resulting data cube were then integrated in velocity using the AIPS task MOMNT, which smooths the data spatially and in velocity before applying a conditional blanking to each channel. Pixels in the original (unsmoothed) cube that correspond to pixels in the smoothed cube with values below a designated level (in this case 1.75 σ) are blanked. The blanked cube, now containing only significant emission, is then integrated to produce three moment maps: the first is the integrated H I flux, the second is the temperature-weighted velocity field, and the third is a map of the velocity dispersions associated with each pixel.

When imaging the CS-configuration data, various weighting schemes were tested to find the optimal combination of resolution (beam size) and sensitivity (single-channel rms). Uniform weighting with a ROBUST factor of −1 produced images with the least degradation in sensitivity (single-channel noise increased by 1.5) for the best increase in resolution (beam size decreased by 1.6). This high-resolution cube has a spatial resolution of $14.''5 \times 13.''1$ and a single-channel rms of 1.26 mJy $beam^{-1}$. As with the D data, the CS data were CLEANed to this 1 σ level, and MOMNT was used to apply a conditional blanking (using a value of 1.4 σ as a cutoff) and to integrate the cube to produce moment maps.

Finally, the edited, calibrated, and continuum-subtracted D and CS data sets were combined in the *u-v* plane to produce a data set with both good resolution ($16.''8 \times 14.''6$) and sensitivity (0.98 mJy $beam^{-1}$). This "C + D" array data set was then Fourier-transformed and CLEANed to the 1 σ level using IMAGR. We used a uniform weighting with a ROBUST factor of −1. Tests were run to determine the optimum value for the integration flux cutoff in MOMNT, and moment maps were produced using a cutoff value of 1.25 σ.

The flux of the C + D data cube was integrated in each channel containing signal over a square 184″ on a side, encompassing the area over which H I is detected in the integrated moment map. The velocity profile is shown and compared with the single-dish observation of Schneider et al. (1990) in Figure 1. The single-dish observation was made with the

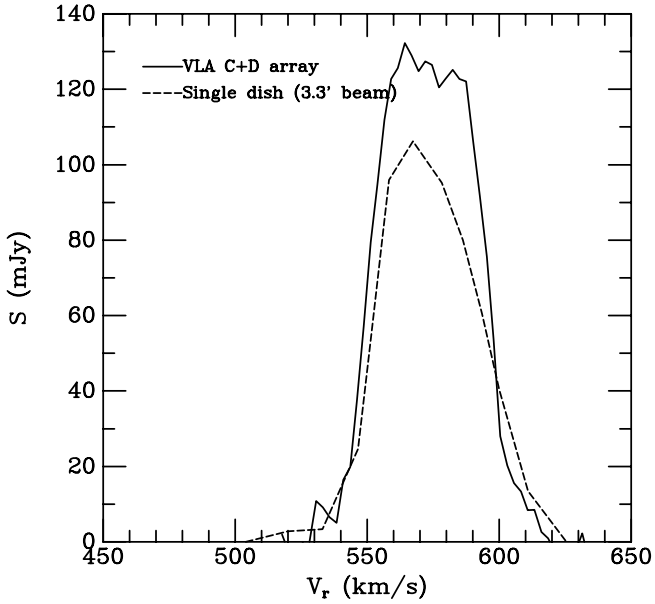

Fig. 1.—Integrated velocity profile made by summing flux over a square ∼3′ on a side from the C+D data. This is compared with the profile obtained with a single-dish radio telescope with a 3.′3 beam by Schneider et al. (1990).

[2] The CS configuration was a modified version of the C configuration, with one antenna moved from the middle of the north arm to a central pad to provide some short spacings. It has since replaced the original C configuration.

TABLE 2
RESULTS OF H II REGION SPECTROSCOPY

Quantity[a]	Region 1	Region 2	Region 3	Region 4	Region 5
R.A. (J2000)	10 47 22.1	10 47 22.8	10 47 23.2	10 47 23.1	10 47 19.8
Decl. (J2000)	14 04 26	14 04 06	14 03 50	14 04 36	14 03 59
Hα/Hβ	2.97 ± 0.55	3.27 ± 0.15	3.00 ± 0.13	2.96 ± 0.22	3.35 ± 0.36
[O III] λ5007/λ4959	2.81 ± 0.08	3.23 ± 0.57	2.90 ± 0.34	2.84 ± 0.08	...
[O II] λ3727/Hβ	2.87 ± 0.93	...	...	...	...
[O III] λ5007/Hβ	1.22 ± 0.06	0.64 ± 0.04	0.60 ± 0.03	1.79 ± 0.08	0.26 ± 0.10
[N II] λ6584/Hα	0.15 ± 0.03	0.14 ± 0.02	0.16 ± 0.04	0.18 ± 0.05	0.15 ± 0.07
[S II] λ6717+6731/Hα	0.13 ± 0.09	0.25 ± 0.07	0.27 ± 0.05	0.53 ± 0.14	0.43 ± 0.30
$E(B-V)$[b]	0.04 ± 0.17	0.13 ± 0.05	0.05 ± 0.04	0.03 ± 0.08	0.16 ± 0.10

NOTE.—Units of right ascension are hours, minutes, and seconds, and units of declination are degrees, arcminutes, and arcseconds.
[a] Line ratios are not corrected for reddening.
[b] This assumes an electron density of 100 cm^{-2}, a nebular temperature of 10^4 K, and the Cardelli et al. (1989) reddening law.

Arecibo telescope and a 3.′3 beam. Thus, the Arecibo beam is comparable to the size of the H I distribution that we detect. Our VLA flux profile has a peak that is 15% higher than the peak from the single-dish data. However, the total integrated flux is actually 5% lower than the corrected flux quoted by Schneider et al. The integrated flux from our D-configuration data alone, which is more sensitive to lower column density emission, is 6.04 Jy km s^{-1}, which is 16% higher than the flux given by Schneider et al. Therefore, it seems that we have recovered all of the flux detected by Arecibo, and perhaps a bit more.

2.2. *Optical Images*

We obtained *UBV* images of DDO 88 using the Lowell Observatory 1.1 m Hall telescope 1999 March and 2000 April. The detector was a SITe 2048 × 2048 CCD. The telescope position was offset 20″ between the three images taken in each filter in order to improve the final flat-fielding. Exposure times of 1800, 1800, and 1200 s for *U*, *B*, and *V*, respectively, were used. The electronic pedestal was subtracted using the overscan strip, and the images were flat-fielded using sky flats. Landolt (1992) standard stars were used to calibrate the photometry. The pixel scale was 1.″13; the seeing was ∼3″. For surface photometry on the DDO 88 images, foreground stars and background galaxies were edited out of the images, and the background sky was fitted with a two-dimensional Legendre function and subtracted.

We also obtained Hα images of DDO 88 during 1995 April with the Perkins 1.8 m telescope at Lowell Observatory. The observations used an 800 × 800 Texas Instruments CCD provided to Lowell Observatory by the National Science Foundation, the Ohio State University Fabry-Pérot (which was used simply as a 3 : 1 focal reducer), an Hα filter with a FWHM of 32 Å, and an off-band filter centered at 6440 Å with a FWHM of 95 Å. The off-band filter was used to subtract stellar continuum from the Hα filter to leave only Hα nebular emission. The Hα exposure was 1800 s. The pixel scale was 0.″49, and the seeing was ∼2.″3. The Hα emission was calibrated using five spectrophotometric standard stars with minimal Hα absorption features (Stone 1977; Oke & Gunn 1983). The Hα filter was also calibrated on other observing runs with spectrophotometry of the H II regions NGC 2363 (Kennicutt et al. 1980) and NGC 604 (Hunter & Elmegreen 2004), and the H II region calibration agreed with the spectrophotometric standard star calibration to 4%. The Hα photometry was corrected for the change in bandpass with temperature and [N II] contamination, although these corrections were small. A standard Anderson Mesa atmospheric extinction coefficient was assumed for Hα.

The *H*-band data were taken on 2003 February 28 at the WIYN Observatory 3.5 m telescope at Kitt Peak National Observatory. The Near-Infrared Imager (NIRIM) was used (Meixner et al. 1999) with a plate scale of 0.″69 pixel^{-1} and a field of view of ∼2.″9 × 2.″9. The data were dark-subtracted and flat-fielded (using dome flats). Source and sky images were taken in an off-on-on-off repeating pattern to enable the removal of atmospheric background emission. The median of the three or four sky images closest in time was subtracted from each on-source image. The individual on-source frames were shifted to align to the nearest half-pixel, and combined. This resulted in a total of 15 minutes on-source integration. The data were calibrated using the only two stars on the image bright enough to be present in the 2MASS catalog,[3] and thus we estimate that the magnitudes are accurate to only ∼30%.

In addition to the *UBVH* and Hα images presented here, *B*, *R*, and Hα images of DDO 88 obtained with the Michigan-Dartmouth-MIT Observatory 1.3 m telescope were discussed by Knezek et al. (1999). We employ those data here as well. See Knezek et al. for details on the reduction of those data.

2.3. *Optical Spectroscopy*

Long-slit spectra were obtained of DDO 88 along three position angles with the Double-Imaging Spectrograph on the 3.5 m telescope at Apache Point Observatory 1998 March 20–22. The spectrograph uses a dichroic and two independent collimators and cameras to allow one to obtain a blue and a red spectrum simultaneously. There were four grating setups used to observe DDO 88, and they have the following wavelength coverages and dispersions:

1. Blue at 4360–5090 Å, 1.55 Å pixel^{-1}; red at 5890–6915 Å, 1.3 Å pixel^{-1}.
2. Blue at 3800–4680 Å, 1.55 Å pixel^{-1}; red at 4500–6230 Å, 1.3 Å pixel^{-1}.
3. Blue at 3600–6420 Å, 6.3 Å pixel^{-1}; red at 3600–8470 Å, 7.2 Å pixel^{-1}.
4. Blue at 3600–6420 Å, 6.3 Å pixel^{-1}; red at 4300–9800 Å, 7.2 Å pixel^{-1}.

A 1.″5 slit was used at position angles of 155.°5, 51.°5, and 124°. Spectrophotometric standard stars were observed to determine the response function, and HeNeAr arc lamps were used to set the wavelength scale.

[3] See http://www.ipac.caltech.edu/2mass.

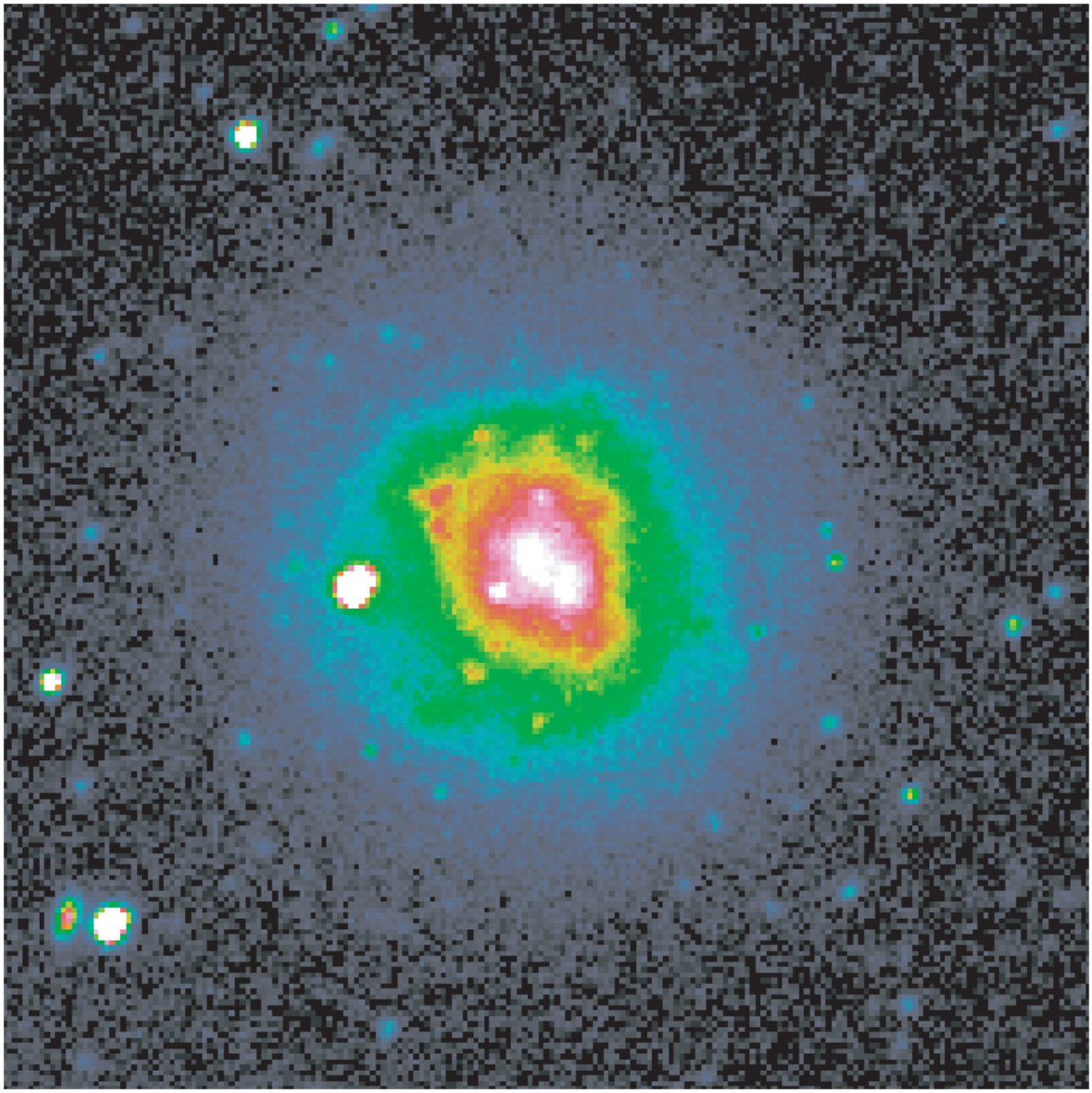

FIG. 2.—False-color representation of the *V*-band image of DDO 88. We show the logarithm of the *V*-band image in order to allow comparison of the inner and outer parts of the galaxy. North is up; east is to the left.

The blue camera used a 512×512 SITe CCD with a scale of $1''.1$ pixel^{-1}, and the red camera used an 800×800 TI CCD with a scale of $0''.6$ pixel^{-1}. The electronic pedestal was subtracted from the two-dimensional images, a bias frame was subtracted, and pixel-to-pixel sensitivity variations were removed using observations of internal continuum lamps. The arc lamps were traced along the slit to map spatial distortions, and the images were linearly repixelized in wavelength. The two-dimensional images were corrected for extinction using the standard extinction function from Kitt Peak National Observatory, then fluxed using the sensitivity function determined from the standard stars; multiple images were combined to remove cosmic rays, and background sky was fitted and subtracted using the part of the slit beyond emission from DDO 88. Finally, the H II regions along the slit were identified, and one-dimensional spectra were extracted.

The emission lines in each one-dimensional spectrum were fitted with Gaussians to determine the flux. The signal-to-noise ratio of a line was taken as the rms of the continuum surrounding the emission line times the FWHM of the line. Several spectra were smoothed to increase the signal-to-noise ratio. Since there is more than one grating setting for each slit position, there are often multiple measurements of a line. In addition, two H II regions were captured on two slit positions. Therefore, the emission-line flux ratios were taken as the average.

Emission-line ratios are given in Table 2. The ratio [O III] $\lambda5007/\lambda4959$ is one diagnostic of the quality of the data. For a nebula with an electron density of 100 cm^{-2} and a nebular temperature of 10^4 K, this ratio should be 2.9. For our H II regions, the ratio is within 1 σ of the expected value. For these same nebular parameters, we determine the $E(B-V)$ from the ratio of Hα to Hβ, using the Cardelli et al. (1989) reddening function.

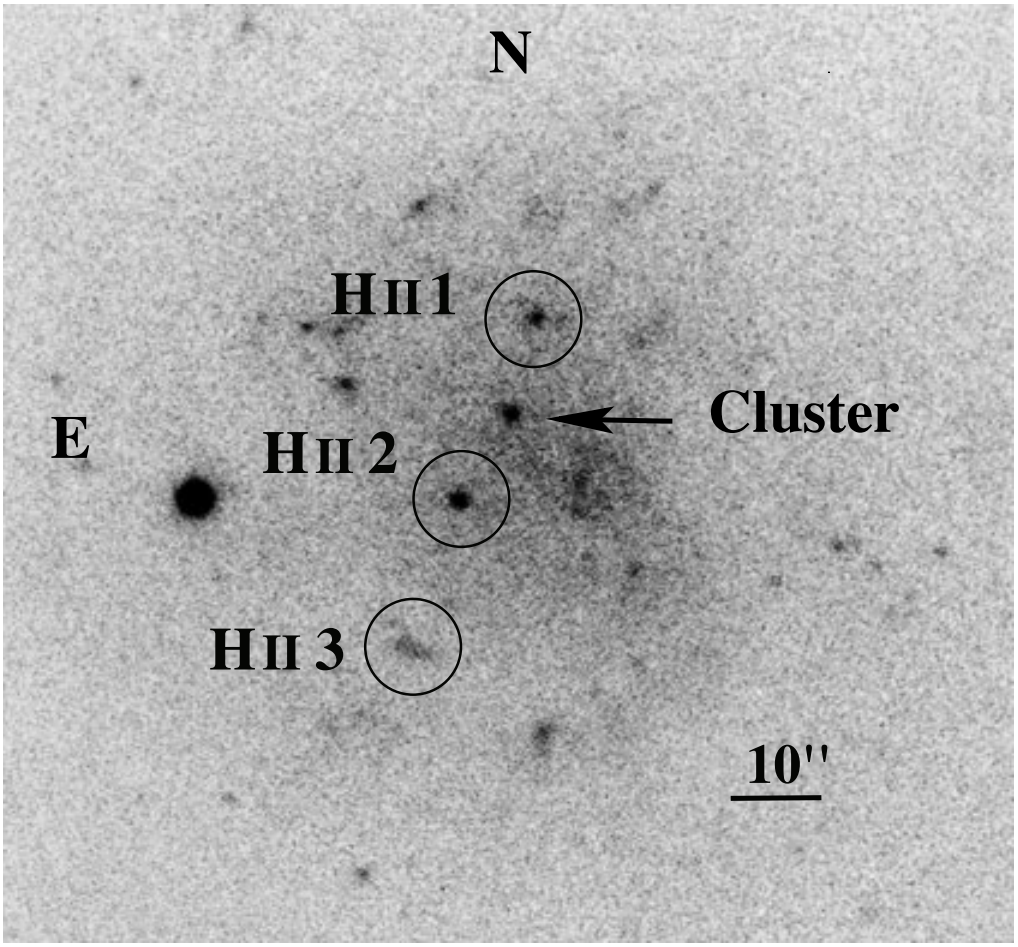

FIG. 3.—Photographic plate image from the Carnegie Atlas (Sandage & Bedke 1994) taken with the Palomar 200 inch using a 103a-O + GG 1 emulsion (4050 Å). The cluster is located in the center of the galaxy, in between two H II regions. North is up; east is to the left.

These values range from 0.03 ± 0.08 to 0.16 ± 0.10, where foreground $E(B-V)_f$ is 0.01. [O II] λ3727 was measured only for one H II region. The method by McGaugh (1991) for determining the oxygen abundance from [O III] $\lambda\lambda$5007, 4959 and [O II] λ3727 yields a value of 7.9 for $12 + \log(\mathrm{O/H})$ if we assume the lower abundance branch and 8.8 if we assume the higher abundance branch. A value of 7.9 would place DDO 88 at the low abundance end of the range for Im galaxies, and a value of 8.8 would be higher than most Im galaxies (Hunter & Hoffman 1999).

3. RESULTS: OPTICAL

3.1. *General Morphology*

Our *V*-band image of DDO 88 is shown in Figure 2. We display the logarithm of the image in a false-color representation so that the reader can see the bright inner parts and the fainter outer parts in one image. We see that DDO 88 changes its shape slightly as it goes from the inner to the outer galaxy, becoming more round in the outer parts. Specifically, we find an ellipticity $(1 - b/a)$ from the minor-to-major axis ratio b/a of 0.13 in the inner galaxy at a *V*-band surface brightness corrected for reddening $\mu_{V,0}$ of 23.7–24.7 mag and an ellipticity of 0.03 in the outer parts at a $\mu_{V,0}$ of 26.2 mag. If the intrinsic $(b/a)_0$ is 0.3 (Hodge & Hitchcock 1966), as is often taken for irregular galaxies, the observed outer b/a implies an inclination of 16°. Thus, the galaxy is observed close to face-on.

In the *V*-band image we can also see an asymmetry at low surface brightness levels. The galaxy appears to be slightly more extended to the north and northwest than to the south and southeast. However, this kind of optical asymmetry is seen in other irregular galaxies (e.g., NGC 2366; Hunter et al. 2001). DDO 88 is located only 15 kpc on the plane of the sky and 93 km s^{-1} radially from the giant elliptical galaxy NGC 3377 (hence DDO 88's alternate name of NGC 3377A). However, except for this small optical asymmetry, we see no signs of disturbance in DDO 88 that could be ascribed to an interaction with this much larger galaxy (NGC 3377 is about 3 mag brighter in *B* than DDO 88).

There is a red object located in the center of the galaxy that is visible in the *H*-band image. Radial profiles on both the *V* and *H* images show that it is extended, so it is probably a star cluster. It is the center of the three bright regions extending from the northwest to the southeast in Figure 3.[4] The other two bright regions bracketing the cluster are H II regions 1 and 2 in Table 2. Region 2, just to the southeast of the cluster, also shows up in the *H* image; it is the only H II region detected in *H*. We have performed multiaperture photometry of both the cluster and the southeast H II region, which is discussed below.

3.2. *Surface Photometry*

UBV and *H* surface photometry are shown in Figure 4. Because the galaxy is nearly face-on, we used circular apertures increasing in radius from 11.″3 to 79.″4 in steps of 11.″3. All

[4] Digitized image obtained from NED; see http://nedwww.ipac.caltech.edu.

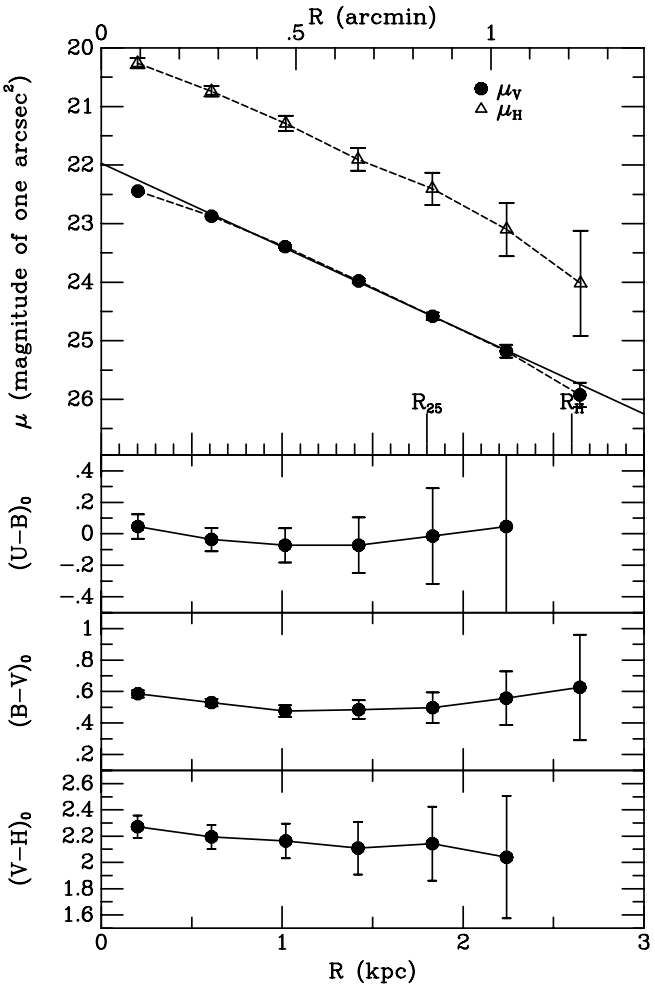

FIG. 4.—*UBVH* surface photometry of DDO 88. The photometry is corrected for an internal reddening $E(B-V)$ of 0.05 mag and an external reddening of 0.01 mag. The exponential fit to the *V*-band surface brightness profile is shown as a solid line.

photometry has been corrected for reddening using a total $E(B-V)_t = E(B-V)_f + 0.05$, where the foreground reddening $E(B-V)_f$ is 0.01 (Burstein & Heiles 1984). We use the reddening law of Cardelli et al. (1989) and $A_V/E(B-V) = 3.1$.

Integrated magnitudes and colors are given in Table 3. We measured an integrated *B* magnitude of 14.00 ± 0.02. This can be compared to a value of 13.97 given by de Vaucouleurs et al. (1991) and 13.95 measured by Knezek et al. (1999), both corrected for extinction using our values. Thus, $M_{B,0}$ is -15.34 ± 0.02 to a radius of 79″. The integrated $(U-B)_0$ is -0.03 ± 0.09 and $(B-V)_0$ is 0.52 ± 0.02. These are within 0.05 and 0.03 mag, respectively, of the values given by de Vaucouleurs et al. (1991). The integrated $(V-H)_0$ is 2.30 ± 0.03, which is similar to NGC 1156 (2.1; Hunter & Gallagher 1985), but redder than NGC 4449 (1.9; Hunter et al. 1999) and NGC 2366 (1.3; Hunter et al. 2001) when measured to comparable radii. The agreement of the integrated colors and magnitudes with other values in the literature gives us confidence in our calibration and photometry. The integrated colors show that DDO 88 lies at the red end of the distribution of a large sample of Im and Sm galaxies in a *UBV* color-color plot (see Fig. 2 of Hunter 1997).

From $\mu_{B,0}$ as a function of radius, we measured R_{25} to be 0.′83 (=1.8 kpc). Our radius is 26% smaller than that given by de Vaucouleurs et al. (1991), but 11% larger than the radius measured by Knezek et al. (1999). The Holmberg radius, $R_{\rm Hol}$, originally defined to a photographic surface brightness, is measured at an equivalent *B*-band surface brightness $\mu_B = 26.7 - 0.149(B-V)$. For a $(B-V)_0$ of 0.5, the Holmberg radius is determined at a $\mu_{B,0}$ of 26.6 mag arcsec^{-2}. We are able to measure $\mu_{B,0}$ only just to the Holmberg radius. We find that $R_{\rm Hol}$ is 1.′2 (=2.6 kpc).

TABLE 3
SUMMARY OF INTEGRATED PROPERTIES

Parameter	Value
D[a]	7.4 Mpc
$E(B-V)_f$[b]	0.01
R_{25}	0.′83
	1.8 kpc
$R_{\rm Hol}$	1.′2
	2.6 kpc
μ_0 (*V*-band)	21.97 ± 0.04 mag arcsec^{-2}
α_V	0.70 ± 0.01 kpc
α_H	0.78 ± 0.02 kpc
$M_{B,0}$ ($r = 79''$)	−15.34 ± 0.02
$(U-B)_0$ ($r = 79''$)	−0.03 ± 0.09
$(B-V)_0$ ($r = 79''$)	0.52 ± 0.02
$(V-H)_0$ ($r = 79''$)	2.30 ± 0.03
log $L_{\rm H\alpha,0}$	38.89 ergs s^{-1}
SFR[c]	0.0055 $M_\odot$ yr^{-1}
log SFR/area[c]	−3.26 $M_\odot$ yr^{-1} kpc^{-2}

[a] $V_{\rm GSR} = 481$ km s^{-1}; $H_0 = 65$ km s^{-1} Mpc^{-1}.
[b] $E(B-V)_f$ is foreground reddening due to the Milky Way (Burstein & Heiles 1984). For the broadband stellar photometry in DDO 88, we assume an additional internal reddening of 0.05 mag; for the H II regions we assume an additional internal reddening of 0.1 mag.
[c] Star formation rate derived from $L_{\rm H\alpha}$ using the formula of Hunter & Gallagher (1986) that integrates from 0.1 to 100 $M_\odot$ with a Salpeter (1955) stellar initial mass function. The area is πR_{25}^2.

We fitted a line to $\mu_{V,0}$ in the inner 17″–62″, and the fit is shown as the solid line in Figure 4. DDO 88 is fitted well with an exponential disk profile having a central *V*-band surface brightness μ_0 of 21.97 ± 0.04 mag arcsec^{-2}. If $\mu = \mu_0 + r/\alpha$, α_V is $0.''326 \pm 0.''005$, or 0.70 ± 0.01 kpc. Our value is low compared with the α_B and α_R of 50″ and 48″ measured by Knezek et al. (1999). De Jong (1996) has determined disk characteristics of a large sample of galaxies spanning a wide range in type. DDO 88 has a central surface brightness, corrected to the *B* passband, that is a little high and a disk scale length that is a little low compared with what de Jong finds for late-type galaxies.

As in most irregular galaxies, colors in DDO 88 are quite constant. Figure 4 indicates that DDO 88 does not exhibit any major color gradient with radius. The slopes of the *V* and *H* surface photometry plots are 0.70 ± 0.01 and 0.78 ± 0.02, respectively. In addition, two-dimensional ratio images confirm what is seen in the azimuthally averaged colors: that there are no regions other than the central cluster and star-forming regions associated with H II regions that are significantly different in color from the rest of the galaxy.

The integrated colors of the central cluster are $(U-B)_0 = 0.41$ and $(B-V)_0 = 0.55$, which are red. This could indicate that the cluster is either old or heavily reddened. Photometry of the nearby H II region (region 2), however, shows no excessive reddening [$(U-B)_0 = -0.30$ and $(B-V)_0 = 0.42$], which is confirmed by the spectroscopy. Reddening in the center of the galaxy near the cluster is therefore modest, so it is likely that the cluster's colors are due to age. We have used the Leitherer et al. (1999) cluster evolutionary models to compute evolutionary tracks for

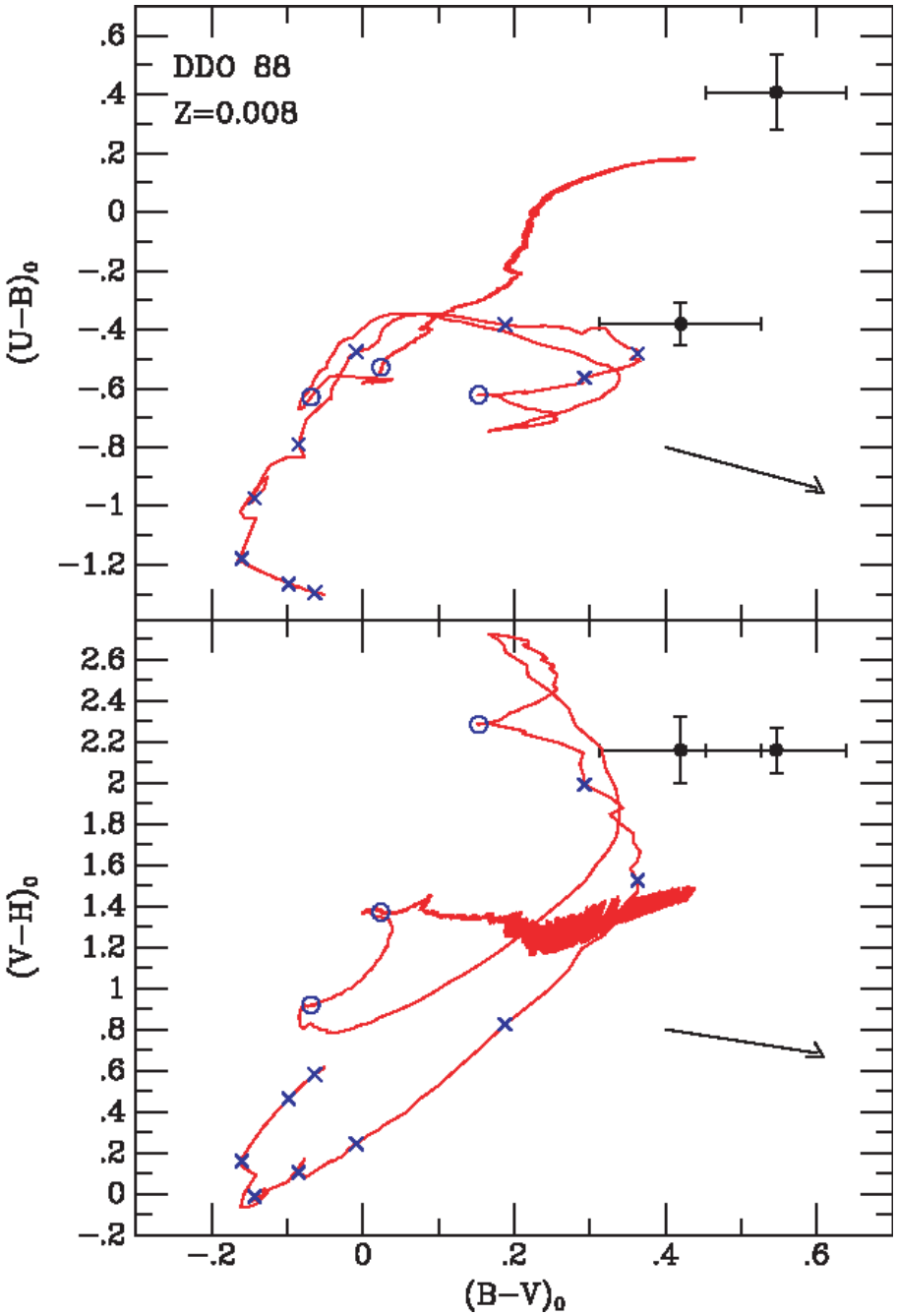

FIG. 5.—Cluster and H II region 2 colors plotted with Leitherer et al. (1999) cluster evolutionary tracks for $Z = 0.008$. The arrows are reddening lines; the photometry has been corrected for modest reddening [$E(B-V) = 0.06$ mag]. The cluster is the redder of the two objects. The crosses mark 1–9 Myr in 1 Myr steps; the circles mark 10, 20, and 30 Myr; the tracks end at 1 Gyr.

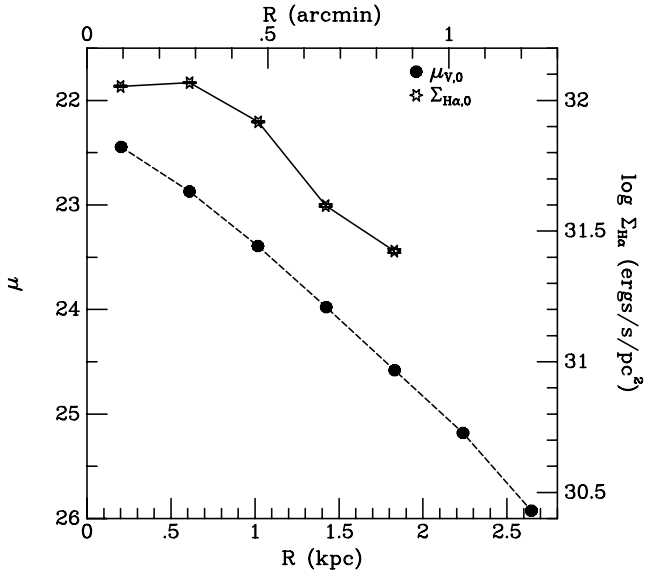

FIG. 6.—Azimuthally averaged Hα surface brightness and reddening-corrected V-band surface brightness. The Hα luminosity is proportional to the star formation rate and was corrected for extinction using an $A_{H\alpha}$ of 0.28 mag. The scales for $\Sigma_{H\alpha,0}$ and $\mu_{V,0}$ have been set so that they cover the same logarithmic interval.

both the cluster and the nearby H II region (region 2) (Fig. 5). The H II region colors are consistent with an age of 7–10 Myr, as expected. The red central cluster colors agree with an age of 1–3 Gyr. This is discussed further in § 5.3.

3.3. *Star-forming Regions*

Figure 1*b* of Knezek et al. (1999) displays a nice color-composite image that shows their Hα image of DDO 88 on broadband B and R images. One can see a modest number of H II regions spread over the galaxy. The farthest distinct H II region is found at a radius of 2.0 kpc from the center of the galaxy. This radius is $1.1R_{25}$, or $0.8R_{\rm Hol}$. The H II regions are quite modest in luminosity. If we take the Hα luminosity of the Orion nebula as 10^{37} ergs s^{-1}, the four brightest H II regions are only 2–6 Orions in luminosity.

The integrated Hα luminosity and inferred star formation rate are given in Table 3. We have corrected the Hα fluxes for reddening assuming an internal $E(B-V)$ of 0.1 mag and an external reddening of 0.01 mag. The total Hα luminosity for the galaxy represents about 80 times that of the Orion nebula. The star formation rate (SFR) is determined from the Hα luminosity using the formula of Hunter & Gallagher (1986), which assumes a Salpeter (1955) stellar initial mass function from 0.1 to 100 $M_\odot$. In order to compare with other galaxies, we normalize the SFR to the size of the galaxy. Here we use the size as defined by R_{25}. The normalized SFR is quite normal compared with other Im and Sm galaxies (see Fig. 7 of Hunter 1997). At its current rate of consumption, the galaxy could turn gas into stars for another 19 Gyr if all of the gas (H I+He) associated with the galaxy can be used. The timescale to run out of gas becomes even longer if recycling of gas from dying stars is also considered (Kennicutt et al. 1994). As Knezek et al. (1999) point out, this galaxy can form stars at this rate for a very long time yet to come. We note that the $L_{H\alpha}$ given by Knezek et al. is a factor of 5 higher than what we measure here. We have not been able to determine the cause of this difference.

In Figure 6, we show the azimuthally averaged Hα surface brightness and compare it with $\mu_{V,0}$. Outside of the center, which is depressed in Hα emission, the Hα surface brightness drops at a rate comparable to that of the starlight. As in most Im and Sm galaxies, the current star formation activity ends before the detected starlight ends. The outer 36% of the galaxy by area in which we detect starlight, as defined by the Holmberg radius, contains no detectable H II region.

4. RESULTS: H I

4.1. H I *Morphology*

Measured H I parameters are shown in Table 4. In the high-sensitivity D-configuration integrated flux map, the diameter of the H I at a column density of 1×10^{19} atoms cm^{-2} is 4.′1 (8.8 kpc). The total H I mass detected in the system is $7.8\times10^7\ M_\odot$. These data lack the resolution to detect any structure in the H I distribution, however, and the map shows essentially circular contours of smoothly increasing density toward the center of the system. The H I contours on the V-band image are shown in Figure 7.

The C+D configuration flux map (Fig. 8), with its decreased sensitivity to low-level emission, can only be measured out to $\sim1\times10^{20}$ atoms cm^{-2}. The diameter at the 1×10^{20} atoms cm^{-2} level, 2.′8 (5.9 kpc), is 32% smaller than that detected in the D-configuration data, as it misses the low-level outer envelope. The higher resolution in this data set is better able to resolve the structure in the higher density H I gas, however. The most striking feature in this flux map is a high-density ring in the H I distribution. Defining the H I ring as the region containing emission at levels greater than 4.5×10^{20} atoms cm^{-2}, it has an outer diameter of 3.4 kpc with an average radial thickness of 0.8 kpc and average column density of 5.5×10^{20} atoms cm^{-2}. The ring contains $2.3\times10^7\ M_\odot$ of H I, which is 30% of the total H I mass as measured from the D-configuration data. This ring surrounds a central depression or hole in the H I that has a diameter of 49″ (1.8 kpc) and apparently surrounds the highest surface brightness region of the optical (V band) emission, as demonstrated in Figure 9. The star cluster is located near the center of the hole but is not visible in this image.

There are several discrete clumps of H I embedded in the ring which are not resolved. The average column density in these knots is about 6×10^{20} atoms cm^{-2}, with peak column densities ranging from 6.6 to 7.3×10^{20} atoms cm^{-2}. The largest knot, in the south part of the ring, contains about $2\times10^6\ M_\odot$. These knots do not appear to coincide with any noticeable optical features in either the V or Hα images. Instead, two of the bright Hα regions (regions 1 and 3) are located on either inside edge

TABLE 4
H I PROPERTIES

Parameter	Value
$M_{\rm H\,I}$[a]	$7.8\times10^7\ M_\odot$
$R_{\rm H\,I}$[a] (arcmin)	2.′1
	4.4 kpc
$M_{\rm H\,I}$[b] in the ring	$2.3\times10^7\ M_\odot$
$M_{\rm H\,I}$[b] in the hole	$5.5\times10^6\ M_\odot$
$R_{\rm hole}$[b]	25″
	0.9 kpc
Width of ring[b]	22′
	0.8 kpc
$R_{\rm ring}$[b]	47″
	1.7 kpc

[a] From D configuration; $D = 7.4$ Mpc.
[b] From C+D configuration.

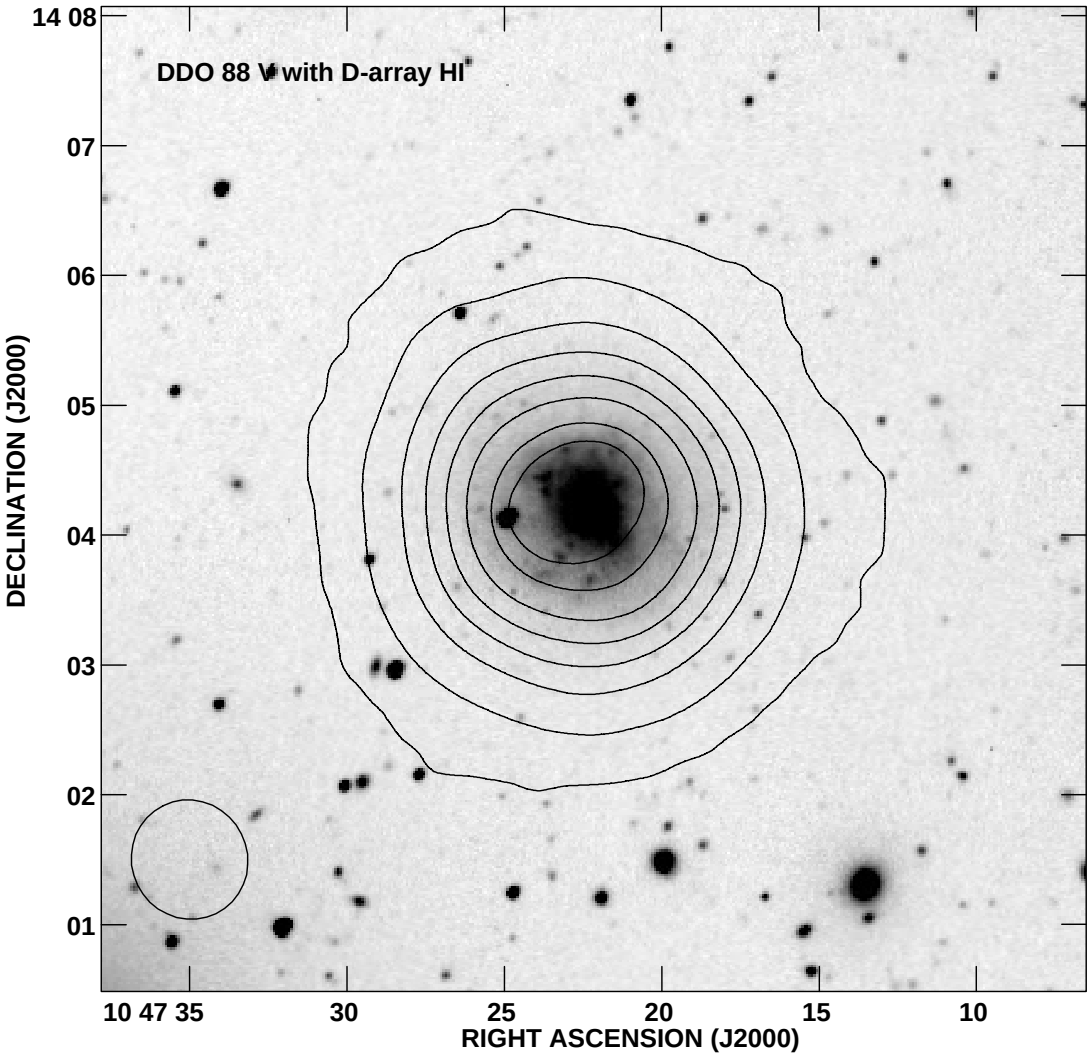

FIG. 7.—*V*-band image with H I contours from the D-configuration flux map. Contour levels are at 0.2, 3.7, 11.1, 18.5, 25.9, 33.3, 40.8, and 44.5×10^{19} atoms cm^{-2}. The size of the beam ($55\farcs6 \times 53\farcs6$) is indicated in the lower left corner.

of the ring in the southeast and the northwest, and the third (region 2) is inside the hole in the H I ring (Fig. 10).

4.1.1. *Surface Density Profile*

In Figure 11, we show the azimuthally averaged surface density of the H I gas in DDO 88. We have integrated the H I in 15″ radial steps using a position angle of 215° and inclination of 28° as determined from the H I kinematics. Along with DDO 88, we plot other irregular galaxies for comparison. From the figure one can see that outside the center (>30″), the gas surface density drops off fairly smoothly. The rate at which the H I drops off with radius is similar to that of other irregular galaxies such as DDO 105 and IC 1613. However, the dropoff is somewhat shallower than that of DDO 50, Sextans A, or DDO 168, but steeper than NGC 2366 or DDO 154. In all, the azimuthally averaged dropoff of the H I surface density with radius appears to be well within the range of what is observed in other irregular galaxies. A central depression in the H I surface density is seen in other galaxies as well, such as IC 1613, Sextans A, NGC 2366, NGC 4449, and possibly DDO 105.

The extent of the H I relative to the optical as measured by R_{25} is a little low compared with the collection of irregular galaxies in Figure 11, but the ratio is the same for DDO 105 and cannot be considered too unusual. In addition the ratio of $R_{\rm H\,I}$ to $R_{\rm Hol}$ in DDO 88 is 1.7, where $R_{\rm H\,I}$ is measured to a column density of 1×10^{19} atoms cm^{-2}. Figure 13 of Hunter (1997) collects $R_{\rm H\,I}/R_{\rm Hol}$ for various irregular galaxies from data in the literature. DDO 88 is seen to lie at the peak in the number distribution.

The overall level of the H I surface density is low compared with that seen in other Im galaxies in Figure 11; DDO 88 is at the low end of the range in peak $\Sigma_{\rm H\,I}$. This may explain why the star formation activity in this galaxy is so modest, although generally there is no correlation between maximum gas surface density and integrated star formation activity in irregular galaxies (Hunter et al. 1998). Furthermore, it is interesting and puzzling that we see H II regions in DDO 88 in the central part of the galaxy, where the H I surface density is even lower. Generally, in Im galaxies the star-forming regions are found where the gas surface density is locally higher than the azimuthally averaged surface density (van der Hulst et al. 1993; van Zee et al. 1997; Meurer et al. 1998; Hunter et al. 2001).

4.2. *Kinematics*

The C+D channel maps (Fig. 12) show H I emission between 541 and 606 km s^{-1}. One can see mostly ordered, largely

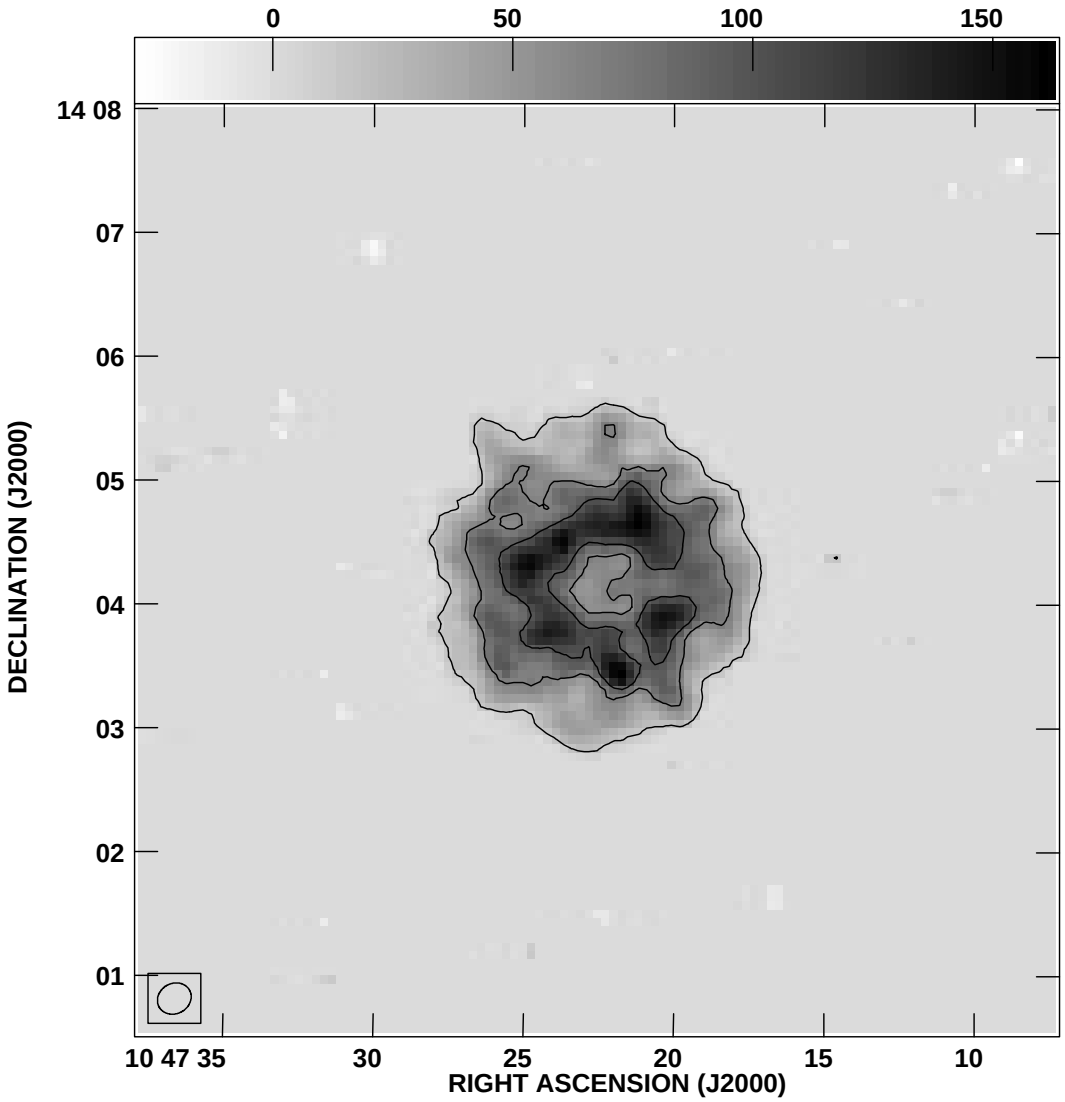

FIG. 8.—Integrated H I flux map from the combined C+D configuration. Contour levels are at 0.7, 3, and 4.5×10^{20} atoms cm^{-2}. The size of the beam ($16\farcs85 \times 14\farcs61$) is indicated in the lower left corner.

solid-body rotation, with "clumps" of H I embedded in low-level gas apparent in each channel. Many dwarf galaxies exhibit solid-body rotation over much of their areas (Swaters 1999), and DDO 88 would seem to be no exception.

4.2.1. *Rotation Curve*

The velocity field of DDO 88 (Fig. 13) clearly shows ordered rotation, so we have fitted a rotation curve to the velocity field. We began by fitting the first-moment map of the C+D data with a Brandt function and allowing all parameters to vary. The fit was reasonable, and from this we fixed the center at $10^{\rm h}47^{\rm m}22\fs52 \pm 0\fs02$, $14^\circ04'10\farcs5 \pm 0\farcs3$. With the center fixed, we fitted a solid-body rotation law to the inner $40''$ radius and determined a systemic velocity $V_{\rm sys}$ of 573.2 ± 0.1 km s^{-1}. Then fixing the center and central velocity, we fitted concentric rings $10''$ wide and in $10''$ steps. First we allowed the position angle, inclination, and radial velocity to vary. We found that the position angle and inclination were fairly constant with radius beyond the inner $20''$ radius, so we determined an average position angle of $215\fdg4 \pm 3\fdg5$ and an average inclination of $28^\circ \pm 8^\circ$. With all but the rotation velocity fixed, we then reran the fits to the velocity field in concentric annuli. We also fitted the velocity field of the D-configuration data alone. The D data are of lower resolution but sensitive to more extended H I emission. To fit the D data, we assumed and fixed the center, $V_{\rm sys}$, P.A., and i determined from the C+D data and solved for the rotation velocity in annuli of $25''$ width.

The final rotation curves for the C+D data and for the D data alone are shown in Figure 14. One can see that the rotation curve from the C+D data rises steeply to a radius of about $20''$ and then rises more shallowly, possibly leveling off at a radius of about $65''$. The maximum rotation speed is 45 km s^{-1} at a radius of $65''$. The rotation curve from the D-configuration data alone rises more gradually and appears to level off around a radius of $90''$, with a maximum rotation speed of 41 km s^{-1}. The shallower rise in the D-configuration rotation curve is undoubtedly due to the large beam size ($55''$) compared with that of the C+D data (beam size of $17''$).

The rotation curve and maximum rotation speed observed in DDO 88 are normal for its luminosity. Figure 1 of Hunter et al. (2000a) plots the maximum rotation speed against M_B for a sample of Im and blue compact dwarf galaxies. With an M_B of -15.3 and a maximum rotation speed of 45 km s^{-1}, DDO 88 lies very close to the ridgeline of the sample. Figure 4:5 of

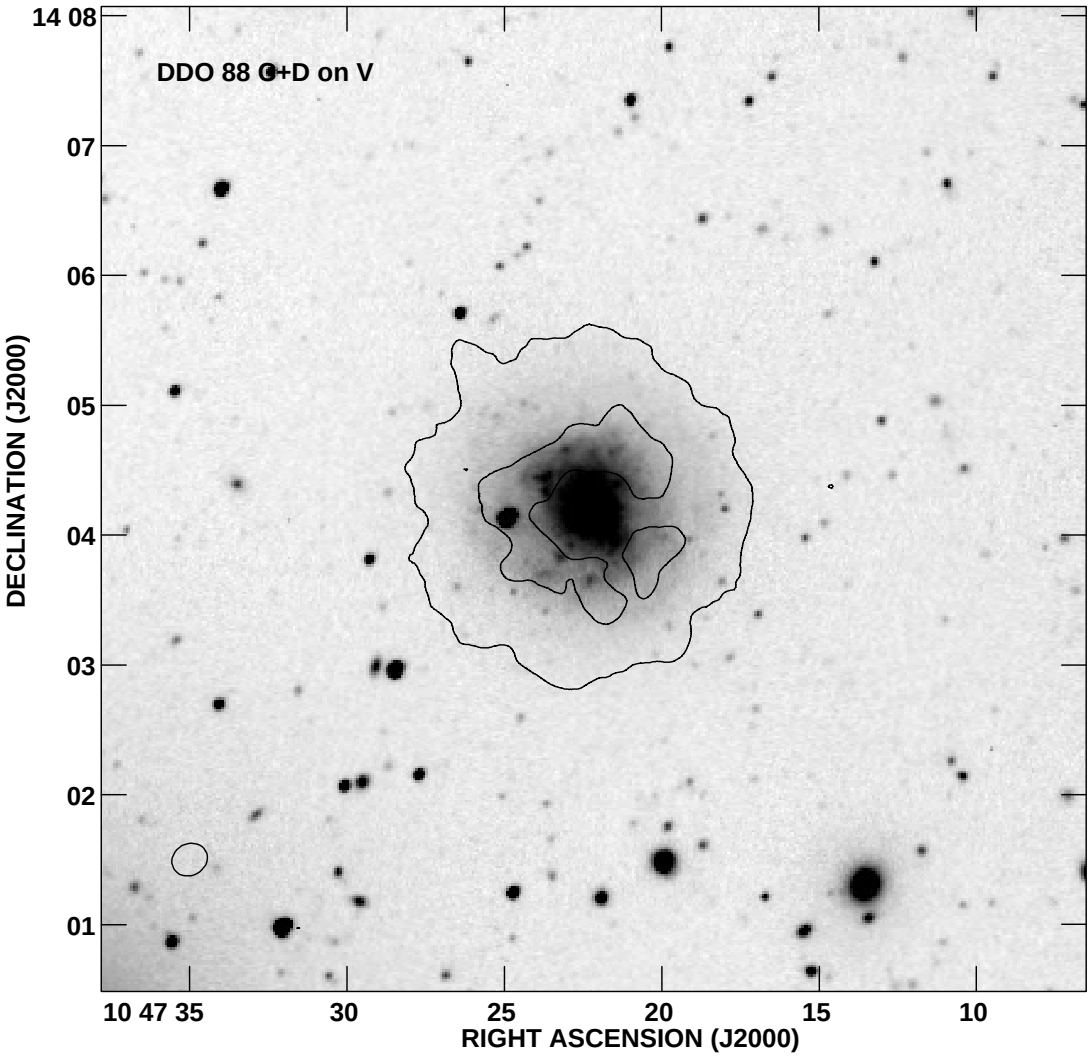

FIG. 9.—*V*-band image with H I contours from the C+D flux map. The contours are at 0.7 and 4.5×10^{20} atoms cm^{-2}. The size of the beam ($16\farcs85 \times 14\farcs61$) is indicated in the lower left corner.

Swaters (1999) shows that the shape of the rotation curve is also fairly normal.

4.2.2. *Velocity Dispersion*

The average velocity dispersion in the second-moment map is on the order of 5 km s^{-1}. On average, the gas dispersions are slightly higher in the area of the ring: 7–9 km s^{-1} versus 4–5 km s^{-1} in the outer regions. There is one notable higher dispersion knot (up to 12 km s^{-1}) located in the southwest (Fig. 15). This high-dispersion region is associated with the brightest H I knot in the ring, but interestingly, it is not associated with any significant optical feature in either the *V* or Hα images. We have fitted Gaussians to the spectra of pixels within the knot; the spectra are shown in Figure 16. Most of the spectra, particularly those located within roughly a beamwidth of the center of the knot, exhibit a central peak with two smaller peaks on either side. Our Gaussian fits indicate that these side components occur at approximately ± 20 km s^{-1} of the central components. The central components have amplitudes of about 6 mJy beam^{-1}, and the side components are roughly half that. The width of the central components average about 13 km s^{-1}, while the side components average 8 km s^{-1}.

The presence of three components could be interpreted as a primary central cloud of gas that contains a shell of gas that is expanding at 20 km s^{-1}. The presence of an expanding shell at that velocity would not be unusual in a star-forming region, nor should it require large numbers of stars to form such a shell. However, we would expect to see Hα emission associated with this kind of star-forming event, which we clearly do not, so this is puzzling. Because we are unable to distinguish whether the shell is expanding or contracting, perhaps instead we are seeing the collapse of what will become a star formation region in the future.

5. DISCUSSION

5.1. *Comparison with Other Holes*

The 3.4 kpc hole in the center of the integrated H I in DDO 88 is what intrigued us about this galaxy. Other irregular galaxies do have holes in their ISM created by the winds and supernova explosions of concentrations of massive stars or by instabilities in the multiphase ISM (Wada et al. 2000). DDO 81 ($M_B = -16.8$) has six holes with diameters greater than 1 kpc, and the largest hole has a diameter of 1.9 kpc (Walter & Brinks 1999). IC 10 ($M_B = -16.5$) has no holes as large as 1 kpc; all are

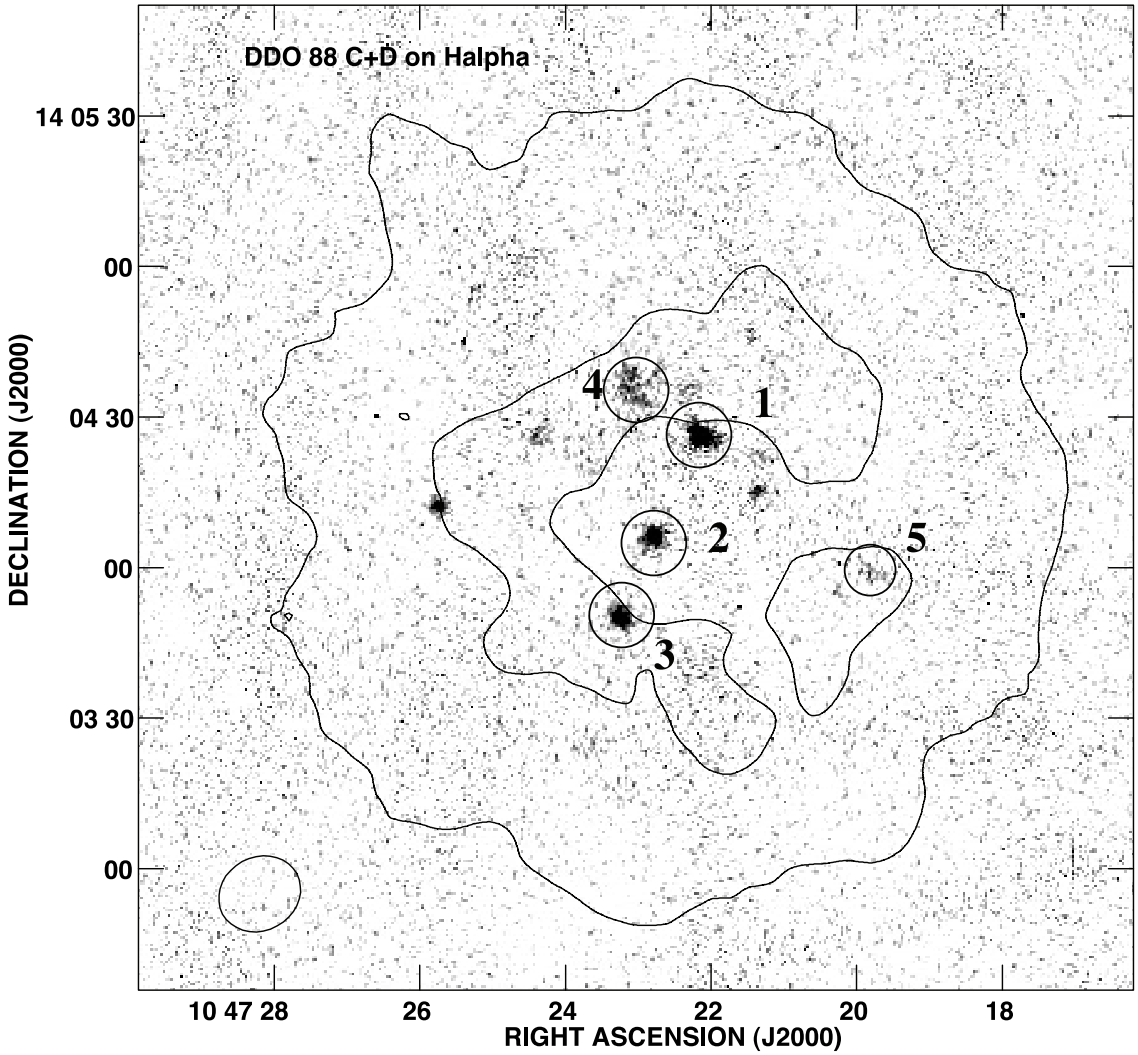

FIG. 10.—Hα image with H I contours from the C+D flux map. The contours are at 0.7 and 4.5×10^{20} atoms cm^{-2}. The size of the beam (16.″85 × 14.″61) is indicated in the lower left corner. The five H II regions listed in Table 2 are labeled. Note that the red cluster is not visible in this image.

100–200 pc in diameter (Wilcots & Miller 1998). Holmberg II ($M_B = -16.6$) has 13 giant ($d \geq 1$ kpc) holes, and the largest is 1.9 kpc in diameter (Puche et al. 1992). Holmberg I ($M_B = -14.6$) has a large hole just south of the center of the galaxy that is 1.2 kpc across (Ott et al. 2001). The tiny M81dwA ($M_B \sim -11$) has a central minimum in its H I that is 960 pc in diameter (Sargent et al. 1983). Thus, DDO 88 is not alone in having such a gas hole. However, holes this large are rare and may be especially unusual in a galaxy of this luminosity.

5.2. *The Central* H I *Minimum*

Here we consider the possibility that the central H I minimum is not a minimum in the gas, but rather that the central H I has been replaced with molecular gas. If this were the case, we can estimate the amount of H I that is "missing" and therefore in the form of H_2. Assuming that the average surface density of H I in the center before any conversion to molecular gas would have been equivalent to that in the ring, we calculated the total H I mass expected before conversion, then subtracted out the amount of H I currently in the minimum. The mass of the "missing" gas is then $3 \times 10^6\ M_\odot$. This mass would correspond to ~10 giant molecular clouds (GMCs) in the Milky Way, where a typical GMC has a mass of $4 \times 10^5\ M_\odot$ (H_2+He) (Scoville & Sanders 1987). To see if this is possible, we consider the consequences of such a large molecular complex: the ratio of molecular to atomic material, embedded star formation, and optical extinction.

Molecular clouds in irregular galaxies are usually part of larger H I complexes (Rubio et al. 1991; Ohta et al. 1993). In the irregular NGC 4449, Hunter et al. (2000b) found that the $M_{H_2}/M_{H\,I}$ is on the order of 0.1–1.8 in the star-forming regions of the galaxy. In DDO 88, if the central region is filled with $3 \times 10^6\ M_\odot$ of molecular gas, for the measured H I mass of $5.5 \times 10^6\ M_\odot$ in the center of the ring, the ratio $M_{H_2}/M_{H\,I}$ is 0.5. If we consider the H I ring to be part of the H I complex that hosts the central molecular complex, the ratio is 0.1. These values are within the range of ratios observed in other irregular galaxies.

If the central region is filled with a large molecular cloud complex, we would reasonably expect it to be forming stars unless it is caught in a very special time. We do see a few small H II regions there, but not at a level that would indicate massive amounts of molecular gas. However, there could be embedded star formation that is not optically visible. If so, such star formation would be detectable in the far-infrared. DDO 88 was not detected by *IRAS*, but observations by *IRAS* do provide upper limits on the far-infrared (FIR) fluxes. These are given by Melisse & Israel (1994) as less than 90 mJy for the flux at 60 μm and less than 130 mJy for the flux at 100 μm. Thus, the FIR

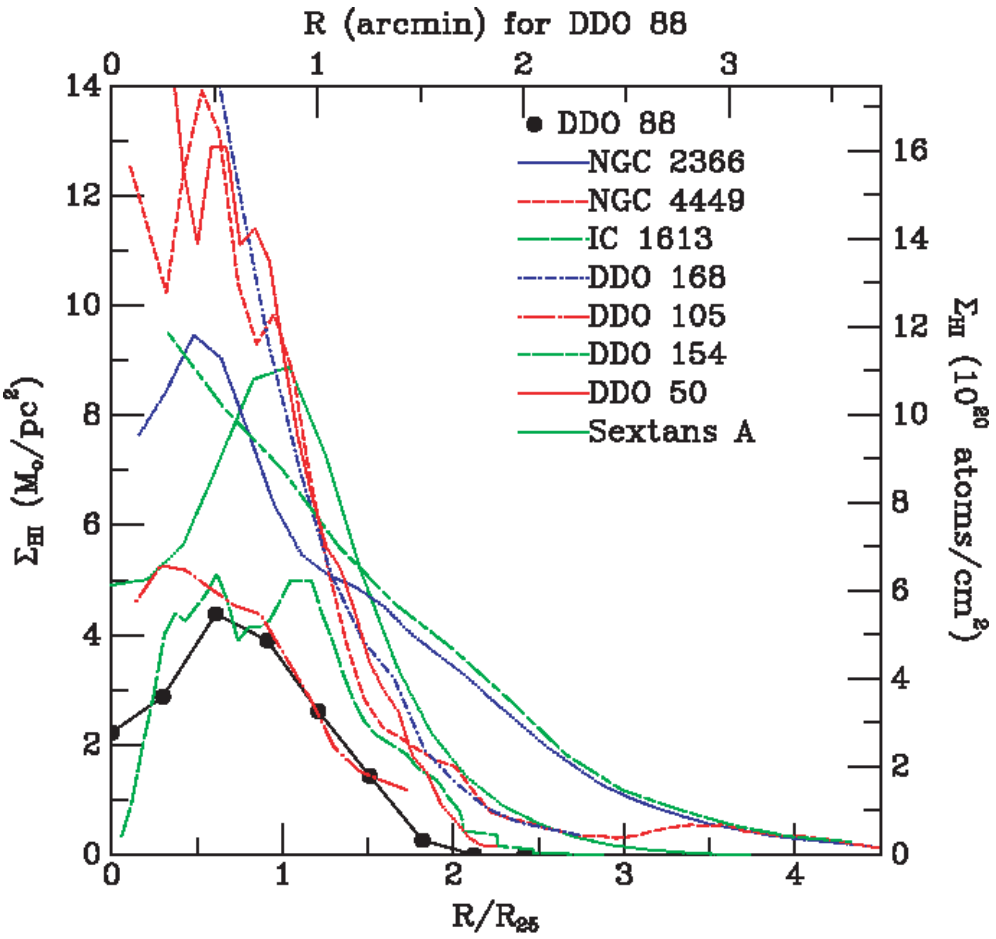

FIG. 11.—Surface density of H I in DDO 88. This is computed in 15″ wide circular rings. We used the position angle (215°) and inclination (28°) determined from the H I kinematics. For comparison, we show the H I surface density profiles of a sample of other Im galaxies (NGC 2366, Hunter et al. 2001; NGC 4449, Hunter et al. 1999; IC 1613, E. Wilcots 2001, private communication; DDO 105 and DDO 168, Broeils 1992; DDO 154, Carignan & Beaulieu 1989; DDO 50, Puche et al. 1992; Sextans A, Wilcots & Hunter 2002).

luminosity $L_{\rm FIR} < 3 \times 10^{40}$ ergs s^{-1}, and $L_{\rm FIR}/L_{\rm H\alpha} < 46$ and $L_{\rm FIR}/L_B < 0.3$. Figure 2 of Hunter et al. (1989) shows a histogram of $L_{\rm FIR}/L_{\rm H\alpha}$ for a collection of Im and Sm galaxies detected by *IRAS*. We see that the upper limit of $L_{\rm FIR}/L_{\rm H\alpha}$ for DDO 88 is normal for irregular galaxies and, because this is an upper limit for DDO 88, the real value could be low compared with these other galaxies. The $L_{\rm FIR}/L_B$ for DDO 88 is already at the low end for irregulars. The values of $L_{\rm FIR}/L_{\rm H\alpha}$ observed for this sample of Im galaxies were interpreted by Hunter et al. as consistent with very little embedded star formation not detected by Hα. Thus, it is unlikely that there is extensive star formation optically shrouded in a central molecular complex in DDO 88.

If the central region is filled with molecular gas, we would also expect the extinction in this region to be much higher than elsewhere in the galaxy. As seen in our Figure 4 and Figure 2*a* of Knezek et al. (1999), the *UBVR* colors in the center of the galaxy are only slightly redder than most of the rest of the galaxy: $U-B$, $B-V$, and $B-R$ are 0.1 mag redder than the bluest annulus in the galaxy. Furthermore, the surface photometry in V is also only slightly (0.2 mag) dimmed in the center relative to the projected fit to the rest of the photometry. Thus, the azimuthally averaged surface photometry of the galaxy does not indicate significant extinction in the center of the galaxy. This is in agreement with the reddening [$E(B-V)$] determined for H II regions in DDO 88 using long-slit spectroscopy; these are given in Table 2. H II region 2 in the table is near the middle of the H I hole. It has an $E(B-V)$ of 0.13 ± 0.05 mag. Foreground reddening is 0.01 mag, so the reddening inside the H II region is 0.12 ± 0.05 mag. This is quite modest, typical of an H II region in an Im galaxy (Hunter & Hoffman 1999), and shows that the H I hole is not heavily reddened.

Thus, we conclude that the central depression in the H I is unlikely to be filled with gas in molecular form. Although the $M_{\rm H_2}/M_{\rm H\,I}$ ratio would not be unusual, the lack of star formation and of significant extinction are not consistent with the presence of a large molecular complex.

5.3. *Formation of the Hole*

If the hole was formed by the action of winds and supernova explosions, what sort of star formation event would be required? The H I ring contains $2 \times 10^7\ M_\odot$, and the hole has an inner radius of 880 pc. We do not detect expansion in the ring, but the background velocity dispersion is 6 km s^{-1}. We will assume that the ring attained its final size when its expansion velocity slowed to the background velocity dispersion. The models of Chevalier (1974) for expansion into a uniform medium give the total energy as $E_s = n_0^{1.12} \times 10^{54}$ ergs for our ring velocity and radius.

From the surface density profile in Figure 11, we can see that the surface density of the H I surrounding the hole is on the order of 5×10^{20} cm^{-2}, and we assume this as the pre-hole

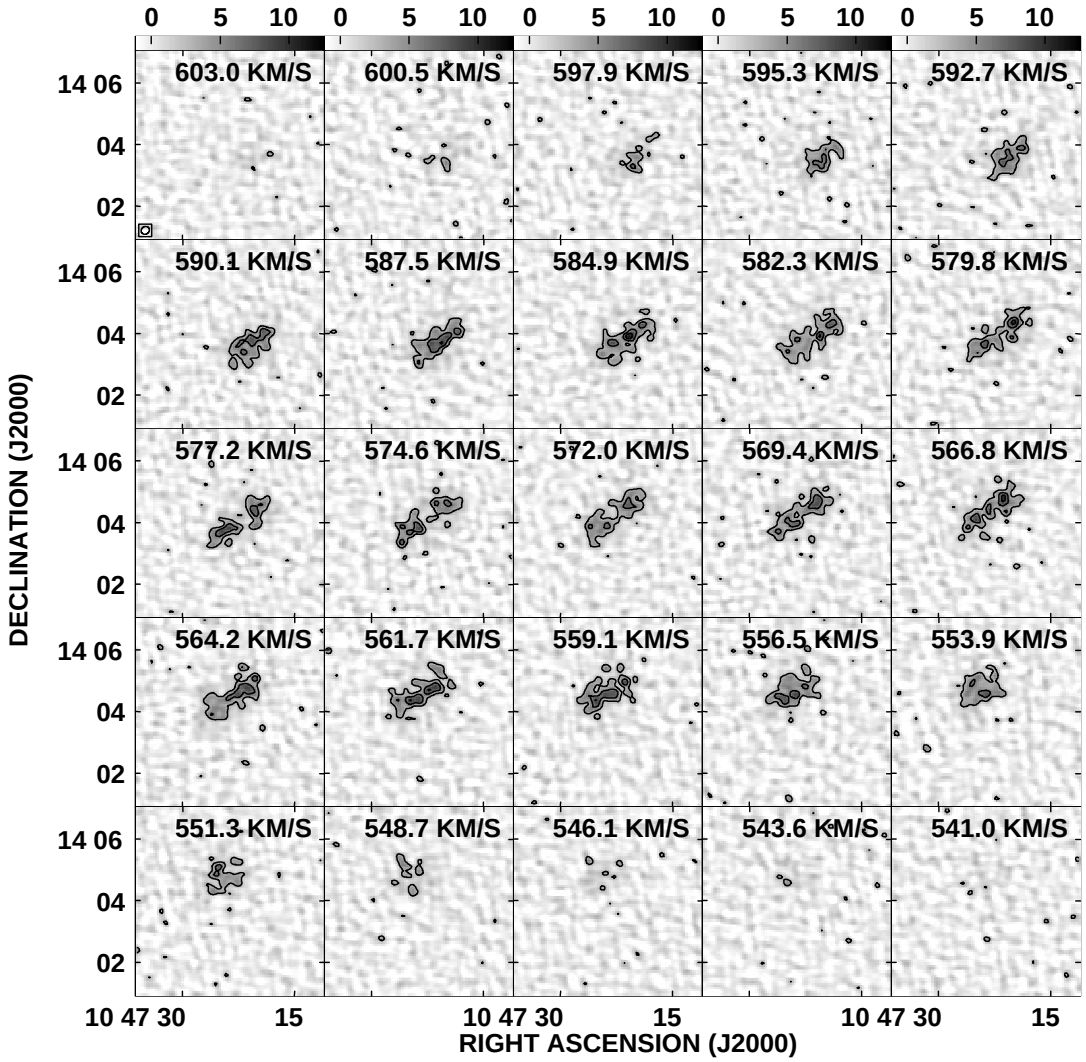

FIG. 12.—H I channel maps from the C+D cube. Contour levels are at 3 (3 σ), 6, and 9 mJy beam^{-1}. The cross indicates the location of the high-dispersion knot.

surface density. The thickness of the galaxy is a harder quantity to estimate. The diameter of the hole, 1.8 kpc, provides a limit. With this thickness, we find that n_0 is 0.1 cm^{-3}. This is probably a lower limit, and we will take an n_0 of 1 cm^{-3} as an upper limit. For 0.1 cm^{-3}, E_s is 1×10^{53} ergs, and for 1 cm^{-3} it is 10 times higher.

With an estimate of E_s we then turn to the shell models of McCray & Kafatos (1987) to solve for N_*, the number of stars with mass greater than 7 $M_\odot$ that formed the shell. If n_0 is 0.1 cm^{-3}, N_* is 1500. For a Salpeter (1955) stellar initial mass function extending from 0.1 to 100 $M_\odot$, the number of O stars (18–100 $M_\odot$) would be 390 and the total mass in stars formed in this event would be 2×10^5 $M_\odot$. If n_0 is 1 cm^{-3}, these numbers would be 10 times higher.

A sanity check is given by NGC 206, a double OB association in M31 that is sitting in an 800 pc diameter H I hole (Brinks 1981). The mass in stars of the OB associations that presumably made the hole is 2×10^5 $M_\odot$ (van den Bergh 1966). Thus, the hole in DDO 88, which is twice the size, would require 1–10 times more mass in stars to form. So, this rough estimate seems reasonable.

What would such a star-forming event mean to the galaxy? We can estimate the total mass in stars in the galaxy from the V-band luminosity ($M_V = -15.8$) if we assume an average mass-to-light ratio. From the models of Larson & Tinsley (1978), the integrated UBV colors of the galaxy are consistent with constant star formation over the past 10 Gyr or a burst 500 Myr ago. Even if the central star-forming event represents a recent burst of star formation, this event is unlikely to have made the bulk of the stars in the galaxy. Therefore, we assume the constant star formation model for which the mass-to-light ratio is 1 $(M/L_V)_\odot$. Thus, the total mass of stars in the galaxy is on the order of 2×10^8 $M_\odot$. This means that the star-forming event required to make the central hole in the H I would have produced of order 0.1%–1% of the total mass of the galaxy, the range representing the two limiting n_0. By comparison, the current star-forming activity is contributing $\sim$0.03% of the galactic mass in stars. Therefore, the star-forming event needed to make the H I hole is 4–40 times higher than the current rate and would represent a modest to vigorous star-forming event in the life of the galaxy.

If the hole was not formed by the action of newly formed massive stars, how then did it form? Wada et al. (2000) have suggested that holes can form in the ISM of galaxies by the nonlinear development of the combined thermal and gravitational instabilities in the disk gas. This does not require the

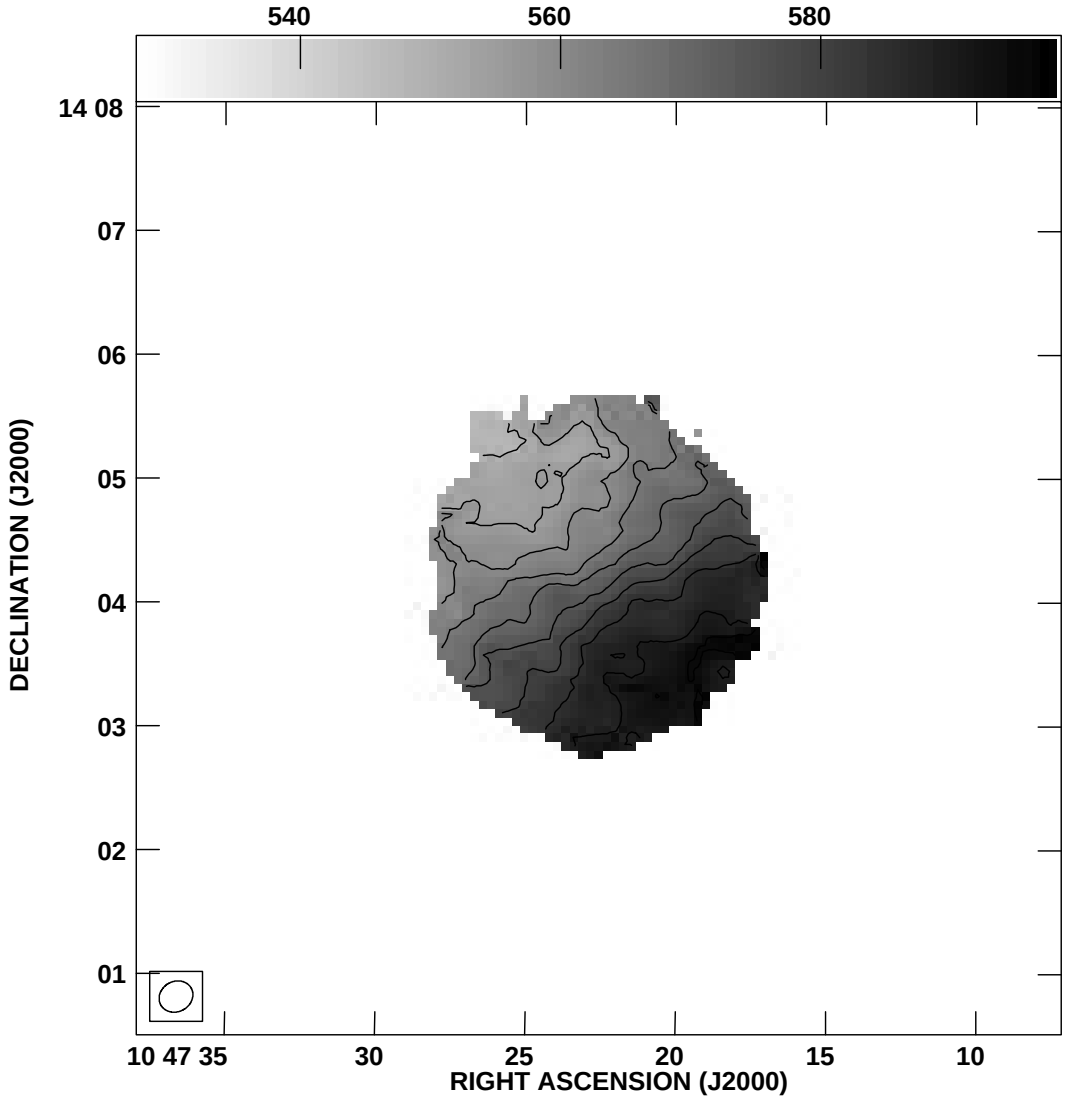

FIG. 13.—Velocity field of H I from the integrated C+D data. Contour levels are every 5 km s^{-1} from 550 to 595 km s^{-1}.

immediate presence of a starburst. This model is used to explain the multitude of holes and filaments found in Im galaxies such as the LMC and DDO 50. In their model a spectrum of sizes of holes is formed, with the typical holes being 500 pc in diameter or less. A few holes of kiloparsec size are formed, but rarely. Thus, the hole in DDO 88 would be an extraordinary event even in their model. Furthermore, there are no other holes in DDO 88—just one big one. This does not really make sense in the context of the Wada et al. models.

Thus, we return to the injection of energy by massive stars longer ago than 0.5 Gyr as the only mechanism for forming the hole in DDO 88 that makes sense. Is the age of the ring consistent with this? Could the red cluster in the center be the remnant of such an event? As we do not detect expansion in our H I data, the ring has apparently stalled. If we assume that expansion stopped when the expansion velocity equaled the dispersion velocity in the gas, this method provides an upper limit to the time it took to *form* the ring. Using a dispersion velocity of 6 km s^{-1} and a size of 880 pc (the inner radius of the hole), this gives us an upper limit of approximately 145 Myr during which the hole and ring were formed. If we use the distance from the center of the hole to the midpoint of the H I ring (1.28 kpc) as our size instead, the maximum expansion time becomes 210 Myr. Note that this does not tell us how long ago the expansion stopped, so in that sense it serves as a rough lower limit to the age of the ring, with the caveat that the ring could also have formed somewhat faster than we have calculated here.

Ott et al. (2001) use a variety of methods to estimate the age of the large stalled H I shell they observed in the low-mass dwarf Holmberg I (Ho I). This shell, which surrounds a depression in the H I just south of the center of the galaxy, dominates the appearance of the galaxy. It extends to approximately half the optical size of the galaxy, similar to what we see in DDO 88. The size of this shell (center to point of maximum H I emission) is 850 pc, which is smaller than the 1.28 kpc for the main ring of DDO 88 but similar to the inner radius of the ring surrounding the hole in DDO 88. Using their shell radius and a background dispersion of 9 km s^{-1}, they estimate a maximum duration of expansion of 90 Myr. This agrees with the total age they find from the central colors using the Leitherer et al. (1999) models, as well as the ages of stars observed in the H I shell itself. They also calculate the age of the shell using a Sedov expansion model (Sedov 1959; Mac Low & McCray 1988; Ehlerová et al. 1997) for the time prior to "break out," when the shell expands out of the disk of the galaxy as defined

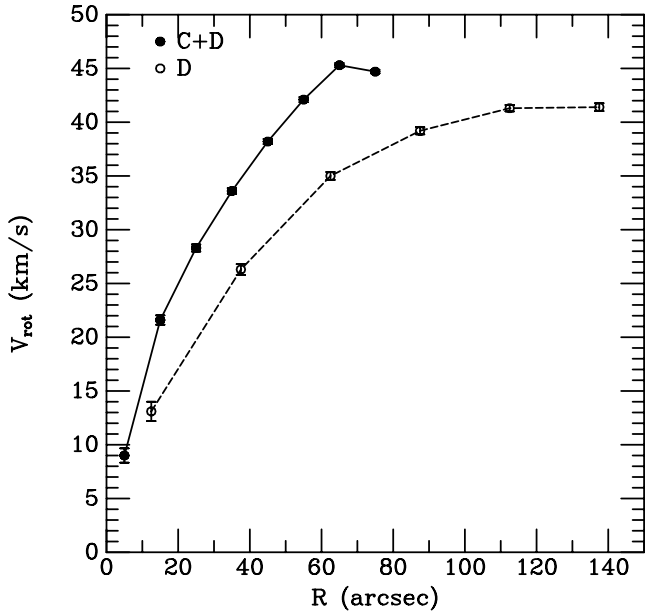

FIG. 14.—Rotation speed as a function of radius, determined from the H I velocity field. The rotation curves are from the C+D data that had a beam size of $16''.85 \times 14''.6$ and from the D-configuration data alone that had a beam size of $55''.6 \times 53''.6$.

by the scale height. After this, the expansion enters a "snowplow" phase (McCray & Kafatos 1987). From this combined shell evolution model, they again come up with an age estimate of approximately 100 Myr.

We also tried applying this shell evolution model to DDO 88. However, there are large uncertainties in calculating or estimating several of the quantities that are used in these equations (eqs. [7] and [8] in Ott et al. 2001). Among these are an estimate of the scale height, which is used as the "critical radius" at which breakout occurs and the time until break out, which depends on this radius as $R_c^{5/3}$. Other parameters used to calculate this "critical time" include the number of supernovae per million years, $\dot{N}$, which depends on the energy required to create the shell and the average energy per supernova, the particle volume density n_0, and the mean molecular mass μ. Both the critical time and the critical radius are then used to estimate the duration of the snowplow phase, with the result depending on $t_c R_c^{-4}$.

Depending on the method we use, we find a scale height for DDO 88 of between 100 and 300 pc. For $\dot{N}$, if we assume (as Ott et al. 2001 did) 10^{51} ergs per supernova, and that they all go off within 40 Myr, then the number of supernova per million years is $E_s/10^{51}/40$. For our $E_s = 10^{53}$–10^{54} ergs (corresponding to $n_0 = 0.1$–1.0 cm^{-3}), this is 100–1000 supernovae, so $\dot{N} = 2.5$–25 Myr^{-1}. As we have used the radius of the hole (not the midpoint of the ring) to calculate E_s, we continue to do so. Thus, for a radius of 880 pc, we find a ring age of 0.5–6.5 Gyr. If instead we use the midpoint of the ring as our ring size, we find a range of 1.4–20 Gyr. Clearly, the upper bound here is unphysical. The lower bounds are in line with the central colors in the hole that indicate no vigorous star formation in the past 0.5 Gyr. The red central cluster colors agree with an age of 1–3 Gyr, so it is old enough to have formed the hole.

Could the ring survive as long as a gigayear, however? The rotation curve indicates that DDO 88 is undergoing primarily solid-body rotation, especially in the inner regions where the ring is located (approximately $30''$–$50''$). Thus, the ring would not be subject to the shearing forces produced by differential rotation. But what about dispersion due to the random motions in the gas? Recall that we have an upper limit for the expansion time of the hole of about 150–200 Myr, so if the ring is more than 0.5 Gyr old, it has been stalled for over 300 Myr. The H I ring has a width of 0.8 kpc. With a dispersion velocity of 6 km s^{-1}, it would take 270 Myr for material to travel twice the width of the ring. This is close to our lowest estimate for the time since the ring stopped expanding. Thus, it would seem that the ring should have undergone at least some, if not total, dispersion if it is much older than 0.5 Gyr. This argues for a younger age for the ring, and against the ring being as old as the red cluster.

The next question is whether the cluster could have produced the required energy. Currently, the cluster has an $M_V = -9.99$. Using the lower age limit of 1 Gyr, we find, according to the Leitherer et al. models, that it would have had an $M_V = -13.6$ at 10 Myr and a mass of $4 \times 10^5\ M_\odot$. This is consistent with the $(2$–$20) \times 10^5\ M_\odot$ of stars that we estimated would have formed in the event that made the hole, and is similar to the mass estimate for the association in NGC 206 (Brinks 1981). This places it in the realm of super star clusters, so it very well could have produced the H I hole from an energy standpoint.

5.4. *Propagating Star Formation?*

Star formation regions have been found at the edges of some H I shells (e.g., Brinks 1981; Walter & Brinks 1999), presumably as a result of instabilities that begin to occur in the swept-up gas from the shell formation (McCray & Kafatos 1987; Elmegreen 1994). Although there is no evidence of increased star formation activity seen from the azimuthally averaged Hα profile (Fig. 6), four of the five Hα regions are associated with the H I ring (Fig. 10). Here, however, we run into an inconsistency if our ring is indeed older than 0.5 Gyr and has been stalled for over 300 Myr. The H II region colors indicate ages of 7–10 Myr, so there would have been a considerable delay between the formation of the ring and the onset of secondary star formation. Would star formation continue to occur in the ring so long after it formed?

There is evidence that secondary star formation resulting from the formation of an H I shell can occur relatively quickly, but how long it continues is much less clear. Walter et al. (1998) observed a still-expanding supershell in IC 2574 with an age of approximately 14 Myr. There are massive H II regions coincident with the rim of this shell, so presumably secondary star formation is occurring now. Constellation III in the LMC has an H I hole 1.4 kpc in diameter that formed about 20 Myr ago, and H II regions with ages of approximately 5 Myr are observed in the shell (Dolphin & Hunter 1998), indicating that it took less than 15 Myr for them to form.

Looking at an older, stalled shell, we turn again to the supershell in Ho I with an age of ~80–100 Myr (Ott et al. 2001). Inside the rim, they observe stars 15–30 Myr old, with younger regions of star formation located on the rim of the hole, so it appears that secondary star formation is occurring some 50–60 Myr after the hole began to form. However, the upper limit on the age of this shell is 90 Myr, so it has been stalled for less than 10 Myr.

Therefore, observed cases of induced star formation give timescales for secondary star formation in the shells of order 60 Myr or less. This leaves us with the problem that the one stellar remnant that we find in the hole is too old, and we cannot identify any younger entity. At this point we see no way around

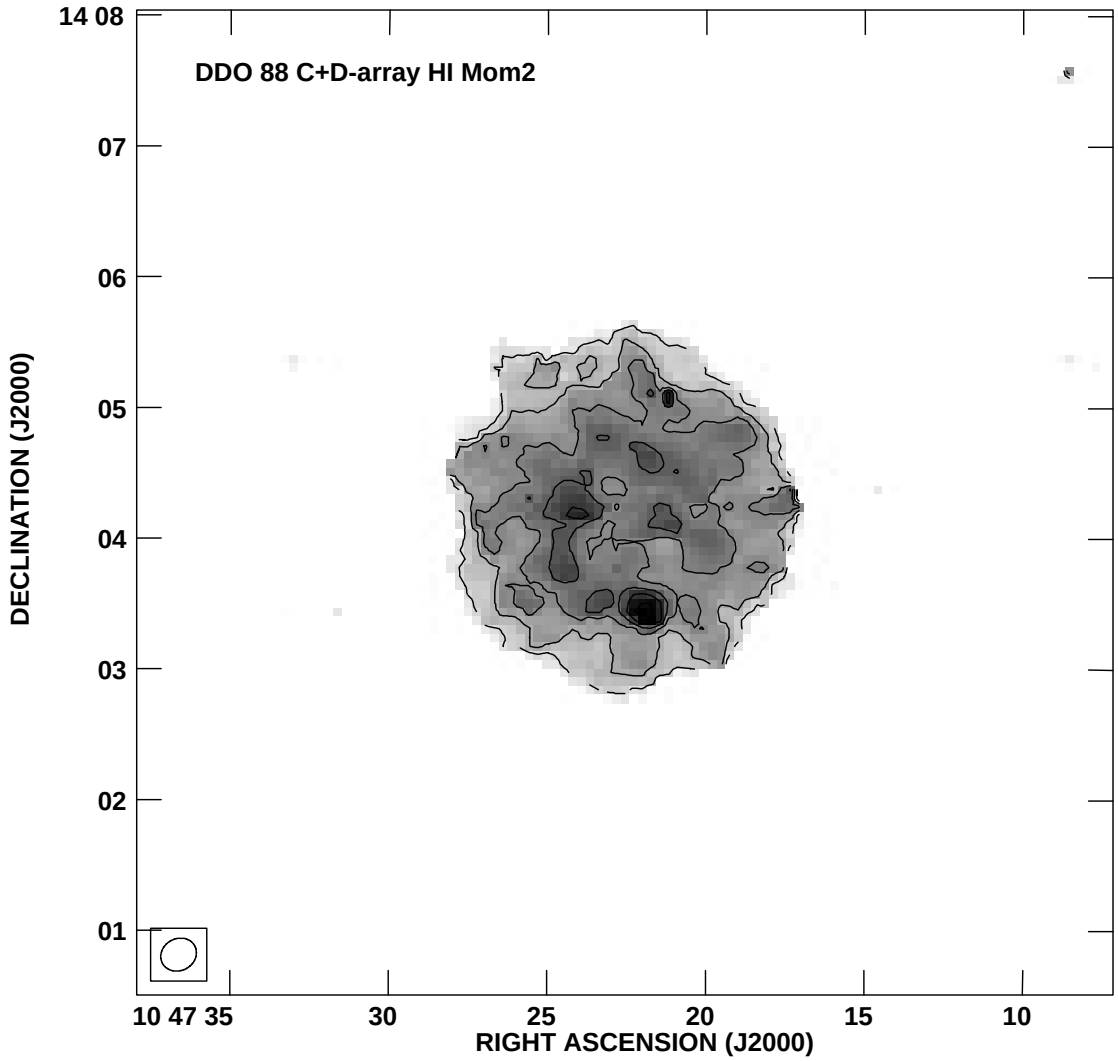

FIG. 15.—Second-moment (velocity dispersion) map from the combined C+D data. Contour levels are 2, 4, 6, 8, 10, and 12 km s^{-1}. The beam size ($16''.85 \times 14''.61$) is indicated in the lower left corner. Note the high-dispersion knot in the southern part of the galaxy.

this inconsistency and cannot clearly point to what has formed a galaxy-sized hole in the gas of this tiny galaxy.

6. SUMMARY

DDO 88 appears to be a fairly normal low-luminosity dwarf galaxy in the optical, with only modest ongoing star formation. There is a slight asymmetry in the outer low-level *V*-band isophotes, but this is not unusual among Im-type galaxies. Its integrated *UBVH* colors put it at the red end of the distribution for Im/Sm galaxies, consistent with the current low level of star formation and suggesting that star formation has been roughly constant over the lifetime of the galaxy. Any significant star formation event would have had to occur more than 0.5 Gyr ago. The azimuthally averaged surface photometry is well fitted by an exponential disk, and there are no major color gradients detected across the disk. These features are typical of Im/Sm galaxies.

In H I, DDO 88's outer regions and global characteristics also appear quite normal. The ratio of H I to optical radius is typical of Im and spiral galaxies. The azimuthally averaged H I surface density is a bit low compared with other irregular galaxies, but it drops off at an average rate.

The normal appearance of the optical and outer regions of the H I gas in DDO 88 give no hint that the center of the galaxy hosts a large (1.8 kpc diameter) H I depression. The H I surrounding the hole is distributed in a high column density ring with an outer diameter of 3.4 kpc. The hole is unusually large for a galaxy of this size, and does not appear to be expanding. If the hole was produced by the energy injection from winds and supernova explosions of massive stars formed in a starburst, the star formation event would have produced $(2–20) \times 10^5\ M_\odot$ of stars, which is 0.1%–1% of the total mass of the galaxy.

There is a red star cluster near the center of the H I hole. Corrected for reddening, evolutionary models give an age of 1–3 Gyr and an initial mass of $4 \times 10^5\ M_\odot$. Both the age and mass are consistent with the cluster being the remnant of a star formation event old enough and energetic enough to have created the H I hole in the center of the galaxy. If this is the case, it is possible that the higher density H I ring surrounding the hole is from gas being swept up and pushed outward by the stellar winds and supernovae that accompanied the cluster formation.

Age estimates for the H I ring indicate that is it likely older than 0.5 Gyr, which might agree with the age of the red cluster, but this is uncertain, as the ring is stalled. An upper limit for the time needed to form the ring is 150–200 Myr. Dispersal time for the ring from random motions in the gas is on the order of 300 Myr, however, which would indicate that this large feature

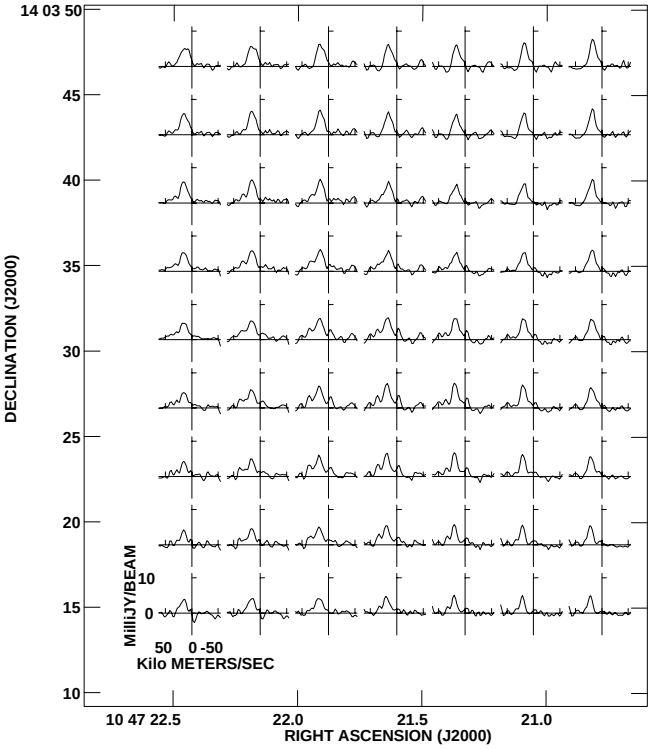

FIG. 16.—Spectra of the high-dispersion knot. Each spectrum is from 1 pixel through the cube. The beam is approximately 4 × 4 pixels.

should have mostly disappeared by now if it is indeed older than 0.5 Gyr. In addition, there are faint H II regions in and on the rim of the ring that are 7–10 Myr old. If they are secondary star formation regions caused by the ring, this also points to a younger ring age. With conflicting evidence regarding how long ago the hole and resultant ring formed, we cannot state that the red central cluster is the causative agent; nor can we rule it out. We have been unable to identify any other mechanism that could be responsible for a such a dramatic feature in this small galaxy.

The authors would like to thank Alan Watson for his help in the acquisition and initial reduction of the IR data, and the referee for helpful comments. Support to D. A. H. for this research came from the Lowell Research Fund and in part from grants AST 98-02193 and AST 02-04922 from the National Science Foundation. This publication makes use of data products from the Two Micron All Sky Survey, which is a joint project of the University of Massachusetts and the Infrared Processing and Analysis Center/California Institute of Technology, funded by the National Aeronautics and Space Administration and the National Science Foundation. This research has made use of the NASA/IPAC Extragalactic Database (NED), which is operated by the Jet Propulsion Laboratory, California Institute of Technology, under contract with the National Aeronautics and Space Administration.

REFERENCES

Brinks, E. 1981, A&A, 95, L1
Broeils, A. H. 1992, Ph.D. thesis, Rijksuniv. Groningen
Burstein, D., & Heiles, C. 1984, ApJS, 54, 33
Cardelli, J. A., Clayton, G. C., & Mathis, J. S. 1989, ApJ, 345, 245
Carignan, C., & Beaulieu, S. 1989, ApJ, 347, 760
Chevalier, R. A. 1974, ApJ, 188, 501
Clark, B. G. 1980, A&A, 89, 377
de Jong, R. S. 1996, A&A, 313, 45
de Vaucouleurs, G., de Vaucouleurs, A., Corwin, H. G., Jr., Buta, R. J., Paturel, G., & Fouqué, P. 1991, Third Reference Catalogue of Bright Galaxies (New York: Springer)
De Young, D. S., & Heckman, T. M. 1994, ApJ, 431, 598
Dolphin, A. E., & Hunter, D. A. 1998, AJ, 116, 1275
Ehlerová, S., Palouš, J., Theis, C., & Hensler, G. 1997, A&A, 328, 121
Elmegreen, B. G. 1994, ApJ, 427, 384
Hodge, P. W., & Hitchcock, J. L. 1966, PASP, 78, 79
Hunter, D. A. 1997, PASP, 109, 937
Hunter, D. A., & Elmegreen, B. G. 2004, AJ, 128, 2170
Hunter, D. A., Elmegreen, B. G., & Baker, A. L. 1998, ApJ, 493, 595
Hunter, D. A., Elmegreen, B. G., & van Woerden, H. 2001, ApJ, 556, 773
Hunter, D. A., & Gallagher, J. S., III. 1985, AJ, 90, 1457
———. 1986, PASP, 98, 5
Hunter, D. A., Gallagher, J. S., III, Rice, W. L., & Gillett, F. C. 1989, ApJ, 336, 152
Hunter, D. A., & Hoffman, L. 1999, AJ, 117, 2789
Hunter, D. A., Hunsberger, S. D., & Roye, E. W. 2000a, ApJ, 542, 137
Hunter, D. A., van Woerden, H., & Gallagher, J. S. 1999, AJ, 118, 2184
Hunter, D. A., Walker, C. E., & Wilcots, E. M. 2000b, AJ, 119, 668
Kennicutt, R., Balick, B., & Heckman, T. 1980, PASP, 92, 134
Kennicutt, R. C., Jr., Tamblyn, P., & Congdon, C. W. 1994, ApJ, 435, 22
Knezek, P. M., Sembach, K. R., & Gallagher, J. S., III. 1999, ApJ, 514, 119
Landolt, A. U. 1992, AJ, 104, 340
Larson, R. B., & Tinsley, B. M. 1978, ApJ, 219, 46
Leitherer, C., et al. 1999, ApJS, 123, 3
Mac Low, M.-M., & Ferrara, A. 1999, ApJ, 513, 142
Mac Low, M.-M., & McCray, R. 1988, ApJ, 324, 776
Martin, C. L. 1998, ApJ, 506, 222
McCray, R., & Kafatos, M. 1987, ApJ, 317, 190
McGaugh, S. S. 1991, ApJ, 380, 140
Meixner, M., Young Owl, R., & Leach, R. W. 1999, PASP, 111, 997
Melisse, J. P. M., & Israel, F. P. 1994, A&AS, 103, 391
Meurer, G. R., Freeman, K. C., Dopita, M. A., & Cacciari, C. 1992, AJ, 103, 60
Meurer, G. R., Staveley-Smith, L., & Killeen, N. E. B. 1998, MNRAS, 300, 705
Ohta, K., Tomita, A., Saitō, M., Sasaki, M., & Nakai, N. 1993, PASJ, 45, L21
Oke, J. B., & Gunn, J. E. 1983, ApJ, 266, 713
Ott, J., Walter, F., Brinks, E., Van Dyk, S. D., Dirsch, B., & Klein, U. 2001, AJ, 122, 3070
Puche, D., Westpfahl, D., Brinks, E., & Roy, J.-R. 1992, AJ, 103, 1841
Rhode, K. L., Salzer, J. J., Westpfahl, D. J., & Radice, L. A. 1999, AJ, 118, 323
Rubio, M., Garay, G., Montani, J., & Thaddeus, P. 1991, ApJ, 368, 173
Salpeter, E. E. 1955, ApJ, 121, 161
Sandage, A., & Bedke, J. 1994, The Carnegie Atlas of Galaxies, Vol. 2 (Carnegie Inst. Washington Publ. 638) (Washington: Carnegie Inst.)
Sargent, W. L. W., Sancisi, R., & Lo, K. Y. 1983, ApJ, 265, 711
Scalo, J., & Chappell, D. 1999, MNRAS, 310, 1
Schneider, S. E., Thuan, T. X., Magri, C., & Wadiak, J. E. 1990, ApJS, 72, 245
Scoville, N. Z., & Sanders, D. B. 1987, in Interstellar Processes, ed. D. J. Hollenbach & H. A. Thronson, Jr. (Dordrecht: Reidel), 21
Sedov, L. I. 1959, Similarity and Dimensional Methods in Mechanics (New York: Academic)
Simpson, C. E., & Gottesman, S. T. 2000, AJ, 120, 2975
Stewart, S. G., et al. 2000, ApJ, 529, 201
Stone, R. P. S. 1977, ApJ, 218, 767
Swaters, R. A. 1999, Ph.D. thesis, Rijksuniv. Groningen
van den Bergh, S. 1966, AJ, 71, 219
van der Hulst, J. M., Skillman, E. D., Smith, T. R., Bothun, G. D., McGaugh, S. S., & de Blok, W. J. G. 1993, AJ, 106, 548
van Zee, L., Haynes, M. P., Salzer, J. J., & Broeils, A. H. 1997, AJ, 113, 1618
Wada, K., Spaans, M., & Kim, S. 2000, ApJ, 540, 797
Walter, F., & Brinks, E. 1999, AJ, 118, 273
Walter, F., Kerp, J., Duric, N., Brinks, E., & Klein, U. 1998, ApJ, 502, L143
Wilcots, E. M., & Hunter, D. A. 2002, AJ, 123, 1476
Wilcots, E. M., & Miller, B. W. 1998, AJ, 116, 2363
Young, L. M., & Lo, K. Y. 1996, ApJ, 462, 203